Author Response for "Single-particle experiments measuring humidity and inorganic salt effects on gas–particle partitioning of butenedial" by A.W. Birdsall et al.

We thank the referees for their thoughtful comments, which have helped improve the manuscript. Our replies are below (referee comment in **bold**, response in normal face, new manuscript content in *italics*, removed manuscript content in ~~strike-through~~).

Referee 1

1) Please clarify the term "effective vapor pressure" – as far as I can tell, it is the vapor pressure that you'd calculate if you assume the activity coefficient to be unity. However, the description on Page 2 lines 15-20 is confusing.

We have updated the description of effective vapor pressure as follows (page 2, line 14):

[…] However in the complex matrix of atmospheric aerosol particles, a compound can instead be thought of as exhibiting an "effective vapor pressure", $P_{\mathrm{vap,eff}}$, meaning the vapor pressure apparently demonstrated by the compound when at equilibrium in a system consisting of a gas phase and single condensed phase, if the role of effects beyond Raoult's Law (i.e., a mole fraction dependence) were ignored. *In particular, the effective vapor pressure describes the vapor pressure that would be calculated if the activity coefficient were unity and condensed-phase chemical equilibria of the compound of interest with other "reservoir" forms were disregarded (see below)*. Similarly, while the Henry's law constant, K_{H}, is used to describe gas–particle partitioning of a compound in a dilute aqueous solution, the behavior of a compound in atmospheric aerosol can be described using an "effective Henry's law constant", $K_{\mathrm{H,eff}}$.

2) Other single particle MS methods have been reported (Jacobs et al. 2018, for example) and should be cited.

The manuscript has been updated (page 5, line 6):

Previous work in our laboratory has developed a technique termed electrodynamic balance–mass spectrometry (EDB-MS) to levitate individual charged droplets with diameter on the order of 10 µm in an electrodynamic balance (EDB) and then measure the droplet's composition with mass spectrometry (MS) (Birdsall et al., 2018). *Other single levitated particle MS methods have been reported (Jacobs et al., 2017).*

3) The height of the pulse is used to quantify the abundance – what happens when you use the area of the pulse? Peak height is much more susceptible to peak shape effects (as evidence by the change in going from 1 Hz to 3 Hz) but peak area may be more robust.

We have previously studied the effect of using peak area versus peak height to quantify the EDB-MS pulse signal. We found that, for systems of various polyethylene glycol oligomers similar to those described in a previous study (Birdsall et al., 2018), there was no appreciable difference in the normalized signal or shot-to-shot signal variability between the two quantification techniques.

4) What is the precision in the spring point method? Asked another way, how reliably can two droplets of a similar size be segregated by size?

Based on a previous study we estimate the precision in the spring point measurement to be ±10% (Birdsall et al., 2018). As discussed in the conclusions of the current manuscript (page 22, line 12), "A measurement of particle diameter with lower uncertainty than the spring point technique would meaningfully reduce the uncertainty in extracted effective vapor pressures, particularly with a continuous diameter measurement. Other research with EDBs has demonstrated the utility of optical sizing techniques for performing this measurement (Zardini et al., 2006)."

5) The PEG is very hygroscopic and will drive the uptake of water at higher RH. It may also effectively hold on to water at low RH, possibly influencing the observations. Were measurements made with pure butenedial to verify if a faster rate of evaporation was observed under dry conditions?

Because our experimental technique requires quantifying butenedial relative to an internal standard, we have found we are unable to collect meaningful data using pure butenedial without any internal standard. However, as noted in Sect. 2.3.1, we did perform experiments in which we measured butenedial evaporation using an alternate internal standard, the C7 dicarboxylic acid diethylmalonic acid. We observed no evidence of a faster butenedial evaporation rate in the presence of diethylmalonic acid.

6) The size of the particle is really key for these measurements given that only one component is evaporating. Typically, vapor pressure measurements are made from looking at the evolving size and then fitting these data to a model. It is unclear in this study why MS was used as the sole measure of the amount of volatile material, when simple light scattering measurements would allow the size change to be resolved with high precision and accuracy. Clearly, for multi-component evaporation, the MS technique would be beneficial.

We agree (and note in the manuscript) the uncertainty in the effective vapor pressures extracted from the set of experiments described in the current manuscript would be reduced with a more precise and accurate sizing measurement. This is capability we plan on adding to this instrumentation. However, using the MS technique we are able to quantify the evaporation rate sufficiently well to reach the scientifically interesting conclusions we describe. Furthermore, measuring the droplet using MS allowed us to check whether the droplet composition in fact remained solely PEG-6 and butenedial, or if other chemistry occurred (e.g., oligomerization). Using the MS technique for these experiments in which the condensed phase is a simple chemical system also will serve as a baseline for future studies based upon the same chemical system with additional condensed-phase chemical processes occurring.

7) Figures 6 and 7 reveal a troubling amount of scatter in the measurement, demonstrating that even using an internal standard, a consistent measure of the composition is not possible. While vague trends are apparent, the uncertainty in the fit must be large. It is not clear if this is accounted for in the reported vapor pressure value. Please clarify. The MS response is not discussed as a source of uncertainty in 3.3, but clearly this is one of the more major sources. Droplets of different radii should exhibit the same relative intensity using the internal standard, so the variation seen in Figures 6 and 7 is an additional factor relating to the response of the instrument.

Though we agree that there is a notable amount of scatter in the data, our results are consistent with the technique measuring a consistent measure of the composition, albeit with a significant source of shot-to-shot noise. In previous work we investigated potential sources of variability and found no systematic explanation (Birdsall et al., 2018). We have revised our fitting technique to better reflect the shot-to-shot variability. The uncertainty windows are now larger, as expected. There is also a somewhat wider confidence interval for the dry evaporation case than the humid, as appears should be the case from the relative noisiness of the data. The manuscript will be updated in the indicated sections with the following descriptions of the revised fitting procedure, along with updated vapor pressures uncertainty estimates obtained as a consequence of following this updated procedure:

Section 2.4 (page 11, line 14):

$P_{\mathrm{vap,eff}}$ of butenedial under each experimental condition was determined by fitting a kinetic model that describes the changing composition of a droplet in time to observations. To determine the uncertainty in the extracted $P_{\mathrm{vap,eff}}$, the analysis considered the uncertainty in the model input parameters and ~~the standard error in the non-linear curve fitting coefficient~~ *the uncertainty introduced by shot-to-shot noise in collected data*, as detailed below. The data consists of a set of individual observations for each trapped and measured droplet, corresponding to a normalized abundance of remaining butenedial (relative to PEG-6) after butenedial evaporation has proceeded for a certain amount of time. Plotting a set of these data points for a single type of experiments shows a decay over time in the normalized butenedial signal~~, which is~~. *The individual data points are binned by time spent in the EDB, and bootstrapped realizations of the binned data are* compared to the kinetic model.

Section 2.4.2 (page 14, line 14):

We used a *combined* Monte Carlo *and bootstrapping* approach to estimate the uncertainty in the retrieved butenedial $P_{\mathrm{vap,eff}}$ due to uncertainties in the other model input parameters. The implementation of the uncertainty analysis is described in Sect. S3. The analysis incorporates the uncertainty associated with model input parameters, including droplet diameter, temperature, scaling factor, and gas-phase diffusivity of butenedial, as reported in Table 2. Using this approach, the per-experiment uncertainties due to uncertainty in model input parameters and ~~standard error in the model fit~~ *shot-to-shot noise in the data* vary by experiment and are reported in Table 3 *as 95% confidence* *intervals* ~~but range between ±20% and ±40%~~. Compared to other uncertainties in our approach, this is likely a dominant source of uncertainty. For comparison, we previously described an uncertainty estimation technique in which we simply considered limiting cases of temperature and diameter parameters to give upper and lower bounds of $P_{\mathrm{vap,eff}}$ of various polyethylene glycols (Birdsall et al., 2018). Using that less detailed uncertainty treatment, which did not consider uncertainty due to measurement variability, the previous estimated *1-σ* uncertainty range was between ±15% and ±25%.

Section 2.4.3 (page 16, line 1):

Because the dominant source of uncertainty in Eq. 4 is $P_{\mathrm{vap,eff}}$, we derive the ~~uncertainty~~ *95% confidence interval* in $K_{\mathrm{H,eff}}$ by using the ~~same relative uncertainty as in~~ *95% confidence interval for* the corresponding $P_{\mathrm{vap,eff}}$.

Section 3.1 (page 16, line 5):

Figure 6 shows data and the corresponding best model fit for the humidity dependence butenedial evaporation experiments. The extracted values for the extracted $P_{\mathrm{vap,eff}}$ of butenedial under the two RH conditions are ~~31.1 ± 9.0 mPa and 39.5 ± 8.8 mPa~~ *28.1 mPa (95% CI 13.1 mPa, 47.8 mPa) and 34.2 mPa (95% CI 18.8 mPa, 54.9 mPa)* for the dry and humid conditions, respectively. (The uncertainty values correspond to a ~~1σ value~~ *95% confidence interval* derived from the *combined* Monte Carlo sampling *and bootstrapping* approach described in the SI, and reflects the uncertainty due to uncertainty in the model input parameters and the ~~standard error of the coefficient in the model fit~~ *shot-to-shot noise in the data*.) We interpret these results to imply $P_{\mathrm{vap,eff}}$ under the dry and humid conditions are indistinguishable, within the uncertainties in our measurements and fitting procedure. […]

Page 18, line 1:

Furthermore the fact that the two $P_{\mathrm{vap,eff}}$ are indistinguishable, at least within the estimated uncertainty ~~of ~30%~~, implies butenedial primarily exists in a hydrated form not only under conditions with a high water content, but also under conditions with lower water content. This observation is also consistent with the collected NMR spectra of butenedial, in which only hydrated butenedial peaks are observed, even under conditions with a lower residual water content. There may be to some degree a shift in equilibrium between the hydrated and non-hydrated forms of butenedial under the different RH conditions, which could lead to a change in $P_{\mathrm{vap,eff}}$, but our results imply any change would correspond to a change in $P_{\mathrm{vap,eff}}$ less than our uncertainty in extracted $P_{\mathrm{vap,eff}}$~~, approximately 20%.~~

Page 18, line 14:

Using Eq. 4 we calculated $K_{\mathrm{H,eff}}$ of butenedial to be ~~$5.2 \pm 1.1 \times 10^{7}$ M atm^{-1}~~ *6.0 (95% CI 3.7, 11) × 10^{7} M atm^{-1}* in the humid, inorganic-free experiment. (Uncertainties in $K_{\mathrm{H,eff}}$ arise from propagating uncertainties in $P_{\mathrm{vap,eff}}$, given the relationship in Eq. 4.) For comparison, $K_{\mathrm{H,eff}}$ of glyoxal has been previously measured to be 4.19×10^{5} M atm^{-1} in an inorganic-free aqueous phase (Ip et al., 2009). The magnitude of the measured $K_{\mathrm{H,eff}}$ for butenedial compared to glyoxal suggests butenedial may have a strong tendency to partition into an available aqueous phase, ignoring the effect of inorganic compounds.

Section 3.2 (Page 18, line 20):

Figure 7 shows data for inorganic salt dependence experiments. For both the sodium chloride and sodium sulfate experiments, the extracted butenedial $P_{\mathrm{vap,eff}}$ is larger than the $P_{\mathrm{vap,eff}}$ measured in the organic-only cases, with values of ~~58 ± 18 mPa and 225 ± 88 mPa~~ *66 mPa (95% CI 36 mPa, 105 mPa) and 169 mPa (95% 71 mPa, 301 mPa)* for the X_{NaCl} of 0.071 and 0.140 sodium chloride experiments, respectively, and ~~172 ± 44 mPa~~ *177 mPa (95% CI 64 mPa, 376 mPa)* for the sodium sulfate experiment. The fact that the $P_{\mathrm{vap,eff}}$ for butenedial becomes higher in solutions containing both inorganic salts, by up to a factor of ~~8~~ *5* under our experimental conditions, implies the inorganic salts in this case have a salting-out effect. [...]

Page 19, line 14

[...] The calculated values of K_{S} using Eq. 5 for the three inorganic experiments are given in Table 3, with uncertainties derived from propagating the uncertainties in the effective Henry's law constants. The K_{S} values for the two NaCl experiments ~~(+0.009 ± 0.032, +0.048 ± 0.021 m^{-1}) have 1σ uncertainty intervals that overlap~~ *(+0.056 (95% CI 0.012, 0.16), +0.074 (95% CI 0.047, 0.15)) have similar values within our uncertainties*. K_{S} for sodium sulfate ~~(+0.073 ± 0.020 m^{-1})~~ *(+0.096 (95% CI 0.056, 0.21))* is ~~approximately three times~~ *somewhat* larger than the K_{S} for sodium chloride in our experiments, *though the confidence intervals largely overlap*. Interestingly, this is a similar trend as previously reported for methylglyoxal in the presence of the same two inorganic salts, of 0.06 m^{-1} and 0.16 m^{-1}, respectively (Waxman et al., 2015). ~~However, the absolute magnitudes of the K_{S} values are measured here to be smaller for butenedial compared to methylglyoxal. This may be due to butenedial having two aldehyde groups that are able to hydrate and have relatively energetically favorable interactions with the inorganic salts, compared to only one aldehyde group for methylglyoxal.~~

Section 4 (Page 21, line 12):

We measured the effective vapor pressure ($P_{\mathrm{vap,eff}}$) of butenedial, under both low (RH<5%) and higher (RH 70%) humidity conditions, to be approximately 30~~-40~~ mPa, which is 4 orders of magnitude lower than the expected vapor pressure of a four-carbon dialdehyde. This result implies butenedial exists primarily in a hydrated form, across a wide range of RH conditions, and the gas–particle partitioning of butenedial in ambient particles favors the particle phase more strongly due to butenedial's hydration. [...]

Figure 6 and caption (Page 16, line 15):

Experiments used to determine the effective vapor pressure of butenedial (BD) in a droplet also containing hexaethylene glycol (PEG-6), under dry (RH<5%) and humid (RH 75 ± 5%) conditions. ~~Points~~ *Small pink points* are observations of individual droplets and the line is the best model fit, as described in the text. *Large points are the mean binned values from the* *bootstrapping procedure, with x error bars showing the width of the bins and y error bars representing a 95% confidence interval of the mean value in the bin, over all bootstrapped realizations. The plotted model fit is for the mean vapor pressure obtained by averaging over all model fits to all realizations.* ~~*with associated*~~ The* vapor pressure ~~and 1σ uncertainty printed~~ *is reported as a 95% confidence interval over repeating the fitting procedure 10000 times*.

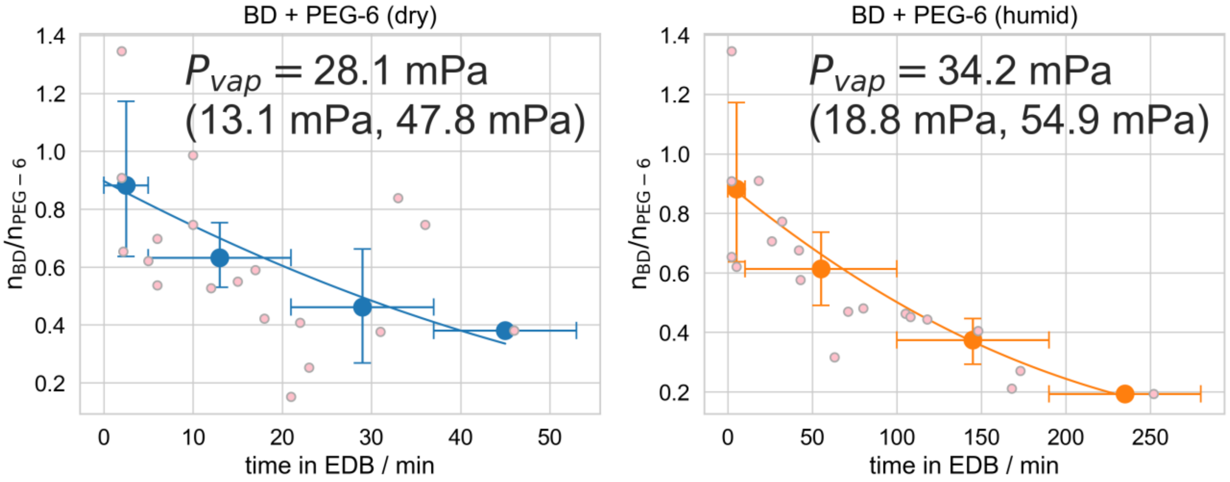

Figure 7 and caption (Page 19, line 1):

Experiments used to determine the effective vapor pressure of butenedial (BD) in a droplet also containing hexaethylene glycol (PEG-6) and either sodium chloride (NaCl) or sodium sulfate (Na_2SO_4), under humid (RH 75 ± 5%) conditions. ~~Points~~ *Small pink points* are observations of individual droplets and the line is the best model fit, as described in the text. *Large points are the mean binned values from the bootstrapping procedure, with x error bars showing the width of the bins and y error bars representing a 95% confidence interval of the mean value in the bin, over all bootstrapped realizations. The plotted model fit is for the mean vapor pressure obtained by averaging over all model fits to all realizations.* ~~with associated~~ *The* vapor pressure ~~and 1σ uncertainty printed~~ *is reported as a 95% confidence interval over repeating the fitting procedure 10000 times*.

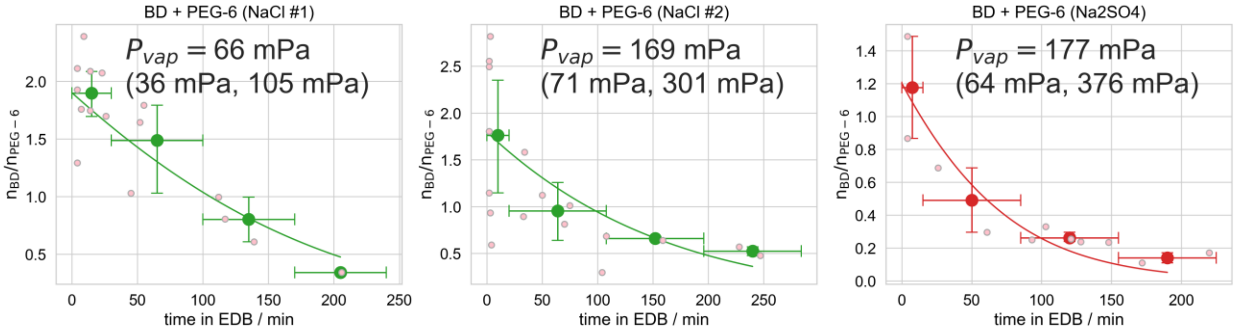

Table 3 caption and contents (Page 15, line 1):

Extracted effective vapor pressures $P_{\mathrm{vap,eff}}$ for butenedial (BD) *with 95% confidence interval bounds (given within parentheses)* obtained from uncertainties in model input parameters described in the main text, along with effective Henry's law constants $K_{\mathrm{H,eff}}$ and Setschenow constants K_{S}, where applicable. Uncertainties in $K_{\mathrm{H,eff}}$ and K_{S} derived from propagating uncertainties in associated $P_{\mathrm{vap,eff}}$ values.

composition	RH	ionic strength (M)	$P_{\mathrm{vap,eff}}(BD, 300K)$ (mPa)	$K_{\mathrm{H,eff}}$ (10^7 M atm^{-1})	K_{S} (m^{-1})
BD + PEG-6	<5%	n/a	*28.1 (13.1, 47.8)*	n/a	n/a
BD + PEG-6	75 ± 5%	n/a	*34.2 (18.8, 54.9)*	*6.0 (3.7, 11)*	n/a
BD + PEG-6 + NaCl (#1)	75 ± 5%	5.3	*66 (36, 105)*	*3.1 (2.0, 5.7)*	*+0.056 (0.012, 0.16)*
BD + PEG-6 + NaCl (#2)	75 ± 5%	9.6	*169 (71, 301)*	*1.2 (0.68, 2.9)*	*+0.074 (0.047, 0.15)*
BD + PEG-6 + Na_2SO_4	75 ± 5%	21.0	*177 (64, 376)*	*1.2 (0.55, 3.2)*	*+0.096 (0.056, 0.21)*

Section S3 (retitled *Combined* Monte Carlo *and bootstrapping* uncertainty analysis) (SI page 4, line 1):

The overall strategy of the *combined* Monte Carlo *and bootstrapping* uncertainty analysis was to obtain a distribution of extracted butenedial vapor pressures was obtained by repeating the fitting procedure in Sect. S1 10000 times, each time using a set of parameter values sampled at random from the set of distributions describing their uncertainties *and an independently generated bootstrapped realization of binned data*. The mean of the extracted butenedial vapor pressures provides a central value for the butenedial effective vapor pressure. The standard deviation describes the uncertainty due to uncertainties in the other model input parameters as well as *shot-to-shot noise in the data* ~~the standard error in the model fit coefficient~~.

The source of the uncertainty in diameter arises from a combination of inherent uncertainty in the measurement and droplet-to-droplet variability, though the characteristics of each droplet were kept as consistent as possible. The uncertainties in gas-phase diffusivity and scaling factor reflect uncertainties in the underlying parameters, rather than reflecting any variability in the values from particle to particle. The uncertainty in temperature does reflect the extent to which the EDB temperature drifted with time, though it should be noted the effect of temperature on the evaporation model over this range is limited. Each input parameter was represented by a Gaussian distribution centered at the mean value and with standard deviation based upon the variability or uncertainty in its measurements. The Monte Carlo approach assumes independence between each of the model input parameters, which is a reasonable assumption for this set of parameters. The distribution of each input parameter was treated separately for each experiment type (i.e., dry, humid, NaCl #1, NaCl #2, Na_2SO_4).

For each type of experiment, we binned the data into different time periods: those for which the time residing in the EDB was approximately 0 minutes, and then a series of equally spaced bins such that a total of 4 time bins were obtained. For each of the 10000 repetitions of the model fitting procedure, a bootstrapping procedure was used within each time bin to generated a bootstrapped realization of the normalized signal response. The model was fit to the mean value of the bootstrapped data within each time bin. The data was scaled for each trial assuming the bootstrapped mean for the "t=0" bin represents the initial normalized molar abundance of butenedial relative to the internal standard.

To calculate $P_{\text{vap,eff}}$ for each iteration of the Monte Carlo technique, a ~~value~~ *95% confidence interval* of a was estimated using the interval that *encompassed the extracted model fit for 95% of the 10000 model fitting trials* ~~accounted for the standard error in the value of a extracted from the curve-fitting procedure. A single value of a was sampled from a standard distribution centered at the optimal estimate of a, arising from the current iteration of curve-fitting procedure, and with standard deviation equal to the square root of the variance of the a estimate, again from the current iteration of the curve-fitting procedure.~~ Using this ~~sampled value~~ *95% confidence interval* of a in Eq. S1, ~~the value of~~ *a 95% confidence interval for* P_{vap} was calculated ~~for a single iteration of the Monte Carlo technique~~.

8) The evaporation rate is proportional to radius-squared, so an uncertainty of up to 50% could lead to an error in vapor pressure by a factor of 4.

As noted in the manuscript and responses above, we agree future experiments will be helped by additional accuracy in the size measurement.

9) I would like to see measurements reported for pure butenedial under dry and high RH conditions. Even if the data is crude due to lack of internal standard, this seems like a key measurement to aid in interpretation of the other data.

Please see our response to point 5, above. Unfortunately, these measurements with the current experimental setup provide no information.

Referee 2

I have little to add to the previous referee comment. I am worried about the unmeasured extent of water evaporation during the "dry" experiment. The panel of Figure 6 that reports on the MS result for the "dry" condition suggests a vapor pressure result (from the shown fit) that is much more precise than I believe, given the data.

We have revised our fitting procedure to better reflect measurement uncertainties, please see response to point 7 of Referee 1.

Scientifically, I wonder about the relationship between the empirical "salting out" that is documented here, with the availability of water for hydration of the aldehyde, given the high demand to solvate the inorganic ions. I suspect this is amenable to modeling, somehow.

Thank you for the interesting suggestion. A future modeling study looking with more detail at the competition you describe between inorganic ion solvation and hydration of the aldehyde would provide helpful insights, but is beyond the scope of the current study.

Co-editor comments

Have you considered the possibility of intramolecular hydrogen bonds forming in the butadiene hydrates (Fig. 2) that would have a significant effect on their volatility and other chemical properties (perhaps also including their propensity to undergo condensation/oligomerization reactions)?

We agree hydrogen bonding may have important effects on volatility and other chemical properties. We will add the following paragraph to the manuscript in the Conclusions (at page 21, line 21):

The formation of intramolecular hydrogen bonds by hydrated butenedial may have a substantive effect on its volatility. Based on the structure of butenedial hydrate, the role of cis/trans isomerism is expected to play a role, with the cis form of butenedial dihydrate more likely to be able to form intramolecular hydrogen bonds and therefore demonstrate a high vapor pressure, compared to the trans form. Though the isomeric form of the precursor (cis) combined with the synthetic mechanism suggest synthesis of purely cis butenedial, evidence from our NMR spectra does not support this conclusion, instead suggesting our experiments were performed with a mixture of cis and trans isomers. However, we do not observe a double exponential shape to our evaporation data, which could imply either the vapor pressures of the cis or trans isomers do not have appreciably different vapor pressures, or the difference in evaporation rates is obscured by the noise in our data. Future studies on a wider set of compounds may help illuminate the effect.

There is a large body of other more recent work that can be discussed and cited regarding the accuracy in particle size that can be obtained from levitated particle trap techniques such as EDB and optical tweezers. The work of Jonathan Reid, Ulrich Krieger, and Ruth Signorell come to mind. A few suggestions:

Steimer, S. S.; Krieger, U. K.; Te, Y.-F.; Lienhard, D. M.; Huisman, A. J.; Luo, B. P.; Ammann, M.; Peter, T. Electrodynamic Balance Measurements of Thermodynamic, Kinetic, and Optical Aerosol Properties Inaccessible to Bulk Methods. Atmos. Meas. Tech. 2015, 8 (6), 2397–2408.

Marsh, A.; Rovelli, G.; Song, Y.-C.; Pereira, K. L.; Willoughby, R. E.; Bzdek, B. R.; Hamilton, J. F.; Orr-Ewing, A. J.; Topping, D. O.; Reid, J. P. Accurate Representations of the Physicochemical Properties of Atmospheric Aerosols: When Are Laboratory Measurements of Value? Faraday Discuss. 2017, 200, 639–661.

Haddrell, A. E.; Davies, J. F.; Reid, J. P. Time-Resolved Measurements of the Evaporation of Volatile Components from Single Aerosol Droplets. Aerosol Science and Technology. 2012, pp 666–677.

Hargreaves, G.; Kwamena, N.-O. A.; Zhang, Y. H.; Butler, J. R.; Rushworth, S.; Clegg, S. L.; Reid, J. P. Measurements of the Equilibrium Size of Supersaturated Aqueous Sodium Chloride Droplets at Low Relative Humidity Using Aerosol Optical Tweezers and an Electrodynamic Balance. J. Phys. Chem. A 2010, 114 (4), 1806–1815.

Gorkowski, K.; Donahue, N. M.; Sullivan, R. C. Emerging Investigator Series: Determination of Biphasic Core–Shell Droplet Properties Using Aerosol Optical Tweezers. Environ. Sci. Process. Impacts 2018, 20 (11), 1512–1523.

These citations will be added to the relevant portion of the conclusion (Page 22, line 12):

This work also helps inform the design of future experimental work using EDB-MS instrumentation. A measurement of particle diameter with lower uncertainty than the spring point technique would meaningfully reduce the uncertainty in extracted effective vapor pressures, particularly with a continuous diameter measurement. Other research with EDBs has demonstrated the utility of optical sizing techniques for performing this measurement (*Gorkowski et al., 2018; Haddrell et al., 2012; Hargreaves et al., 2010; Marsh et al., 2017; Steimer et al., 2015;* Zardini et al., 2006).

Miscellaneous updates

Due to an editing error following two passages were mistakenly omitted from the discussion paper and will be included:

Page 12, line 7:

… where X_i is the particle-phase mole fraction of species i, $P_{\mathrm{vap}_i,\mathrm{eff}}$ is the pure component vapor pressure of species i at temperature T inside the EDB, and k is the Boltzmann constant. *Because the droplet surface is curved, the vapor pressure of a compound above a charged levitated droplet could conceivably be elevated due to the Kelvin effect. The particle charge also could lower the vapor pressure of a compound with a significant dipole moment. However, following Sect. C1 of Huisman et al. (2013) to calculate the combined Kelvin and charge stabilization effects, we conclude the effects are negligible considering the particle diameter and charge for these experiments.*

Page 13, line 24:

The mole fraction of water in the particle, X_{H_2O}, was assumed to be fixed over the entire course of the experiment, ~~assuming~~ *which is true if* the activity coefficient of water does not change appreciably as butenedial evaporates from the particle. *We checked the validity of the assumption by using AIOMFAC to compare the change in calculated* X_{H_2O} *for the humid, inorganic-free experiment, between its initial composition and composition after all butenedial evaporated. We found the change in calculated* X_{H_2O} *to be approximately 0.005, implying the effect of this assumption on our results is negligible within other sources of uncertainty.*

The Acknowledgments section has been updated (Page 23, line 1):

This material is based upon work supported by NSF grant CHE 1808084, the National Science Foundation Graduate Research Fellowship under grant numbers DGE 1144152 and DGE 1745303, and the Harvard University Faculty of Arts and Sciences Dean's Competitive Fund for Promising Scholarship. The authors thank Ulrich Krieger *and Steven Wofsy* for useful discussions.

References

Birdsall, A. W., Krieger, U. K. and Keutsch, F. N.: Electrodynamic balance–mass spectrometry of single particles as a new platform for atmospheric chemistry research, Atmos. Meas. Tech., 11, 33–47, doi:10.5194/amt-11-33-2018, 2018.

Gorkowski, K., Donahue, N. M. and Sullivan, R. C.: Emerging investigator series: Determination of biphasic core–shell droplet properties using aerosol optical tweezers, Environ. Sci.: Processes Impacts, 20, 1512–1523, doi:10.1039/C8EM00166A, 2018.

Haddrell, A. E., Davies, J. F., Yabushita, A. and Reid, J. P.: Accounting for Changes in Particle Charge, Dry Mass and Composition Occurring During Studies of Single Levitated Particles, J. Phys. Chem. A, 116, 9941–9953, doi:10.1021/jp304920x, 2012.

Hargreaves, G., Kwamena, N.-O. A., Zhang, Y. H., Butler, J. R., Rushworth, S., Clegg, S. L. and Reid, J. P.: Measurements of the Equilibrium Size of Supersaturated Aqueous Sodium Chloride Droplets at Low Relative Humidity Using Aerosol Optical Tweezers and an Electrodynamic Balance, J. Phys. Chem. A, 114, 1806–1815, doi:10.1021/jp9095985, 2010.

Ip, H. S. S., Huang, X. H. H. and Yu, J. Z.: Effective Henry's law constants of glyoxal, glyoxylic acid, and glycolic acid, Geophys. Res. Lett., 36, L01802, doi:10.1029/2008GL036212, 2009.

Jacobs, M. I., Davies, J. F., Lee, L., Davis, R. D., Houle, F. and Wilson, K. R.: Exploring chemistry in microcompartments using guided droplet collisions in a branched quadrupole trap coupled to a single droplet, paper spray mass spectrometer, Anal. Chem., 89, 12511–12519, doi:10.1021/acs.analchem.7b03704, 2017.

Marsh, A., Rovelli, G., Song, Y.-C., Pereira, K. L., Willoughby, R. E., Bzdek, B. R., Hamilton, J. F., Orr-Ewing, A. J., Topping, D. O. and Reid, J. P.: Accurate representations of the physicochemical properties of atmospheric aerosols: When are laboratory measurements of value?, Faraday Discuss., 200, 639–661, doi:10.1039/C7FD00008A, 2017.

Steimer, S. S., Krieger, U. K., Te, Y.-F., Lienhard, D. M., Huisman, A. J., Luo, B. P., Ammann, M. and Peter, T.: Electrodynamic balance measurements of thermodynamic, kinetic, and optical aerosol properties inaccessible to bulk methods, Atmos. Meas. Tech., 8, 2397–2408, doi:10.5194/amt-8-2397-2015, 2015.

Waxman, E. M., Elm, J., Kurtén, T., Mikkelsen, K. V., Ziemann, P. J. and Volkamer, R.: Glyoxal and methylglyoxal Setschenow salting constants in sulfate, nitrate, and chloride solutions: Measurements and Gibbs energies, Environ. Sci. Technol., 49, 11500–11508, doi:10.1021/acs.est.5b02782, 2015.

Yu, G., Bayer, A. R., Galloway, M. M., Korshavn, K. J., Fry, C. G. and Keutsch, F. N.: Glyoxal in aqueous ammonium sulfate solutions: Products, kinetics and hydration effects, Environ. Sci. Technol., 45, 6336–6342, doi:10.1021/es200989n, 2011.

Zardini, A. A., Krieger, U. K. and Marcolli, C.: White light Mie resonance spectroscopy used to measure very low vapor pressures of substances in aqueous solution aerosol particles, Opt. Express, 14, 6951–6962, doi:10.1364/OE.14.006951, 2006.

Single-particle experiments measuring humidity and inorganic salt effects on gas-particle partitioning of butenedial

Adam W. Birdsall[1], Jack C. Hensley[2], Paige S. Kotowitz[3*], Andrew J. Huisman[3**], Frank N. Keutsch[1,2,4]

[1]Department of Chemistry and Chemical Biology, Harvard University, Cambridge, MA, USA
[2]School of Engineering and Applied Sciences, Harvard University, Cambridge, MA, USA
[3]Chemistry Department, Union College, Schenectady, NY, USA
[4]Department of Earth and Planetary Sciences, Harvard University, Cambridge, MA, USA
[*]now at: nanoComposix, San Diego, CA, USA
[**]now at: Gentex Corporation, Zeeland, MI, USA

Correspondence to: Adam Birdsall (abirdsall@g.harvard.edu), Frank Keutsch (keutsch@seas.harvard.edu)

An improved understanding of the fate and properties of atmospheric aerosol particles requires a detailed process-level understanding of fundamental factors influencing the aerosol, including partitioning of aerosol components between the gas and particle phases. Laboratory experiments with levitated particles provide a way to study fundamental aerosol processes over timescales relevant to the multiday lifetime of atmospheric aerosol particles, in a controlled environment in which various characteristics relevant to atmospheric aerosol can be prepared (e.g., high surface-to-volume ratio, highly concentrated or supersaturated solutions, changes to relative humidity). In this study, the four-carbon unsaturated compound butenedial, a dialdehyde produced by oxidation of aromatic compounds that undergoes hydration in the presence of water, was used as a model organic aerosol component to investigate different factors affecting gas–particle partitioning, including the role of lower-volatility "reservoir" species such as hydrates, time scales involved in equilibration between higher- and lower-volatility forms, and the effect of inorganic salts. The experimental approach was to use a laboratory system coupling particle levitation in an electrodynamic balance (EDB) with particle composition measurement via mass spectrometry (MS). In particular, by fitting measured evaporation rates to a kinetic model, the effective vapor pressure was determined for butenedial and compared under different experimental conditions, including as a function of ambient relative humidity and presence of high concentrations of inorganic salts. Even under dry (RH<5%) conditions, the evaporation rate of butenedial is orders of magnitude lower than what would be expected if butenedial existed purely as a dialdehyde in the particle, implying an equilibrium strongly favoring hydrated forms and the strong preference of certain dialdehyde compounds to remain in a hydrated form even under lower water content conditions. Butenedial exhibits a salting-out effect in the presence of sodium chloride and sodium sulfate, in contrast to glyoxal. The outcomes of these experiments are also helpful in guiding the design of future EDB-MS experiments.

1 Introduction

Atmospheric aerosol particles contribute significantly to health and climate effects (Boucher et al., 2013; Cohen et al., 2017). In order to understand and predict the extent and composition of aerosol particles across all environments, models of atmospheric aerosol require well-constrained experimentally derived parameters describing aerosol behavior over their entire multiday lifetime in the atmosphere.

One key process is gas–particle partitioning, meaning a quantitative measure of what fraction of a given atmospheric chemical species exists in the gas compared to the particle phase under a given set of atmospheric conditions. For example, accurate understanding of gas–particle partitioning is necessary to understand to what extent a given compound contributes to aerosol particle loading in a particular environment. Despite seemingly being a straightforward question to answer, reconciling observations of gas–particle partitioning with scientists' best understanding of the involved compounds remains an area of active research (Bilde et al., 2015).

The vapor pressure of a compound is an important parameter affecting its gas–particle partitioning behavior, but is not necessarily sufficient to completely describe the partitioning. Strictly speaking, a vapor pressure describes the equilibrium between pure condensed- and gas-phase forms of a particular compound. However in the complex matrix of atmospheric aerosol particles, a compound can instead be thought of as exhibiting an "effective vapor pressure", $P_{\mathrm{vap,eff}}$, meaning the vapor pressure apparently demonstrated by the compound when at equilibrium in a system consisting of a gas phase and single condensed phase, if the role of effects beyond Raoult's Law (i.e., a mole fraction dependence) were ignored. In particular, the effective vapor pressure describes the vapor pressure that would be calculated if the activity coefficient were unity and condensed-phase chemical equilibria of the compound of interest with other "reservoir" forms were disregarded (see below). Similarly, while the Henry's law constant, K_{H}, is used to describe gas–particle partitioning of a compound in a dilute aqueous solution, the behavior of a compound in atmospheric aerosol can be described using an "effective Henry's law constant", $K_{\mathrm{H,eff}}$.

Researchers have used global-scale chemical transport models to investigate the effect of representation of $K_{\mathrm{H,eff}}$ on modeled secondary organic aerosol (SOA) concentrations. In particular, $K_{\mathrm{H,eff}}$ has been used as a parameter describing the loss of gas-phase oxidized semivolatile organic compounds (SVOC) via wet deposition, as a pathway competing with SOA formation. In these modeling studies, one approach has been to use a single uniform $K_{\mathrm{H,eff}}$ of 10^3 to 10^5 M atm^{-1} for SVOC for which $K_{\mathrm{H,eff}}$ is otherwise unknown (e.g., Pye and Seinfeld, 2010). An alternate approach has been to obtain a model-derived parameterized dependence of $K_{\mathrm{H,eff}}$ on volatility that distinguishes between anthropogenic and biogenic precursors (Hodzic et al., 2014). Overall, calculated secondary organic aerosol loadings have been shown to depend on the representation of $K_{\mathrm{H,eff}}$ (Hodzic et al., 2016; Knote et al., 2015), underlining the importance of an improved fundamental understanding of how $K_{\mathrm{H,eff}}$ depends on the chemical behavior of a compound within the complex matrix of atmospheric aerosol particles.

To this end, this research article focuses on two possible effects on $P_{\mathrm{vap,eff}}$ and $K_{\mathrm{H,eff}}$: formation of condensed phase "reservoir" species and nonideality in the condensed phase due to interactions with inorganic ions (Fig. 1).

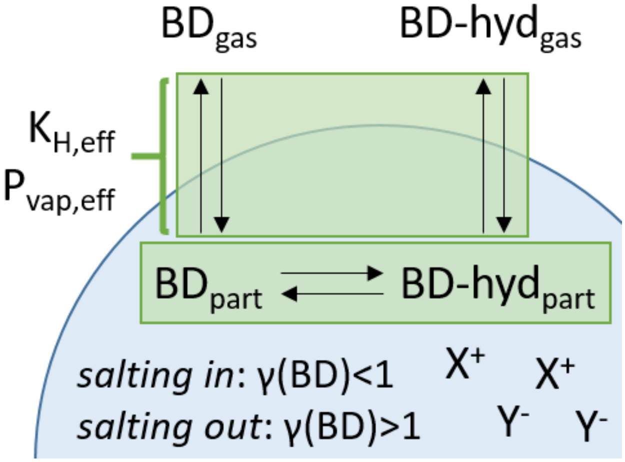

Figure 1: Schematic illustrating the meaning of effective vapor pressure, $P_{\mathrm{vap,eff}}$, and effective Henry's law constant, $K_{\mathrm{H,eff}}$. A compound partitioning between the gas and particle phase (here, butenedial, BD) can exist in the gas phase (BD_{gas}). In the particle phase the compound can exist in its standard form (BD_{part}) but also in fast equilibrium with a "reservoir" species via reversible chemical equilibrium (here, hydrated butenedial, BD-$\mathrm{hyd}_{\mathrm{part}}$). The reservoir species also can partition to the gas phase (BD-$\mathrm{hyd}_{\mathrm{gas}}$), but with a lower vapor pressure. The formal vapor pressure and Henry's law constant of butenedial are related to the equilbrium between BD_{gas} and BD_{part} alone. In contrast, $P_{\mathrm{vap,eff}}$ and $K_{\mathrm{H,eff}}$ are related to the equilibrium between the gas phase and the combined particle-phase abundance of both BD and reservoir species BD-hyd. Additionally, $P_{\mathrm{vap,eff}}$ and $K_{\mathrm{H,eff}}$ can be modulated by the presence of inorganic ions in the particle phase, shown here as generic cations X^+ and generic anions Y^-, which may have a salting-in or salting-out effect.

First, the compound may experience a second equilibrium in the condensed phase with a "reservoir" species with a lower vapor pressure. This reservoir species may be formed by chemical reactions such as hydration or oligomerization. If a large proportion of the compound exists in the form of the reservoir species, the result would be a lower $P_{\mathrm{vap,eff}}$ or higher $K_{\mathrm{H,eff}}$, whose value can depend on both the gas–particle partitioning equilibrium as well as on the equilibrium with the reservoir species (Ervens and Volkamer, 2010). The prototypical molecule for this process is the two-carbon dialdehyde glyoxal, which is known to exist largely in hydrated form in the presence of condensed-phase water, leading to a large $K_{\mathrm{H,eff}}$ (Ip et al., 2009). The process here of reversible formation of a reservoir species is in contrast to the nonreversible formation of a product that takes place in the process of reactive uptake, for example by the isoprene epoxydiols (Lin et al., 2012).

A second effect could be if nonideal mixing, within a single phase, between the compound of interest and other aerosol components causes the activity coefficient of the compound, γ, to differ strongly from unity. Here $P_{\mathrm{vap,eff}}$ or $K_{\mathrm{H,eff}}$ differs from the value in a corresponding ideal mixture by a factor of γ. When the nonideality is due to interactions with inorganic compounds, which can be highly concentrated in ambient aerosol particles, the effect is called a “salting-in” (γ<1) or “salting-out” (γ>1) interaction, depending on whether the interaction favors or disfavors, respectively, the presence of the compound in the phase in question. The effect of salting in or salting out on chemical systems with atmospheric relevance has been assessed with both experimental and theoretical approaches (Toivola et al., 2017; Wang et al., 2014; Waxman et al., 2015; Yu et al., 2011).

The gas–particle partitioning behavior of a given compound will depend on its chemical properties. In the present work we have studied the four-carbon unsaturated dialdehyde butenedial. Butenedial has been observed in the atmosphere and can be produced as a first-generation oxidation product of aromatic compound precursors (Birdsall and Elrod, 2011; Dumdei and O’Brien, 1984; Shepson et al., 1984). Furthermore we are interested in butenedial in terms of what its behavior reveals about the behavior of aldehydic compounds present in the atmosphere. One characteristic of butenedial is that the aldehyde functional groups are expected to readily hydrate under aqueous conditions, such as in an aqueous aerosol phase whose water content is governed by the relative humidity (RH) of the surrounding gas phase (Fig. 2). The properties of butenedial, such as $P_{\mathrm{vap,eff}}$ or $K_{\mathrm{H,eff}}$, are expected to vary greatly depending on whether butenedial primarily exists in a hydrated or non-hydrated form, as has been observed for glyoxal. Another dicarbonyl compound, the three-carbon compound methylglyoxal, has also received appreciable study (e.g., Curry et al., 2018), though one notable structural difference is it contains one aldehydic group and one ketone. Unlike for glyoxal and methylglyoxal, $P_{\mathrm{vap,eff}}$ or $K_{\mathrm{H,eff}}$ for butenedial previously has not been measured experimentally, to the best of our knowledge. Measurement of the gas–particle partitioning of butenedial provides further insight into the behavior of dicarbonyl compounds larger than glyoxal and methylglyoxal.

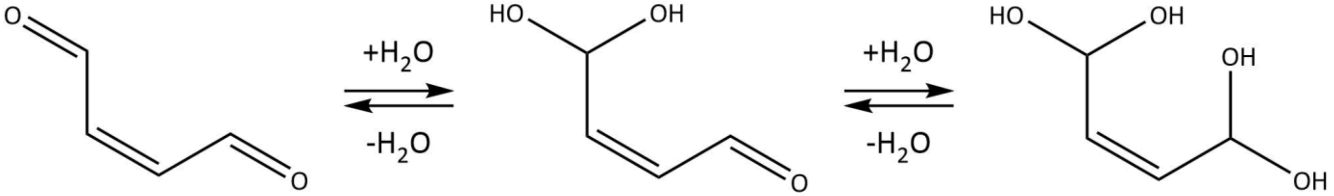

Figure 2: Butenedial (left) in equilibrium with its singly (center) and doubly (right) hydrated forms. The cis isomers of butenedial and its hydrates are shown here but no assumptions are made about the geometric isomer studied in this work.

One approach to address these questions is via laboratory experiments studying individual particles levitated in a chamber surrounded by a bath gas. The advantages of this approach include the ability to isolate and quantify individual processes of interest under controlled conditions. An additional strength of levitated particle experiments is the ability to create a system that exhibits certain key characteristics of atmospheric aerosol: a relatively high surface-area-to-volume ratio enabling investigation of the interaction between bulk and multiphase processes, a condensed phase that can achieve highly concentrated or supersaturated conditions that are often present in atmospheric aerosol particles, and the ability to levitate particles over time scales consistent with their multiday atmospheric lifetimes so that "slow" processes can be studied. Furthermore, the ability to flow a pure bath gas continually through the levitation chamber simplifies the system compared to analogous experiments performed in an environmental chamber, removing the need for continual gas-phase measurements and reducing the set of multiphase processes that need to be accounted for, such as the effects of a more complex gas-phase matrix. The observations made in levitated particle experiments can, with care, be extrapolated to ambient atmospheric conditions, for example, by accounting for the difference in size (and hence surface-area-to-volume ratio) between laboratory and atmospheric particles.

Previous work in our laboratory has developed a technique termed electrodynamic balance–mass spectrometry (EDB-MS) to levitate individual charged droplets with diameter on the order of 10 μm in an electrodynamic balance (EDB) and then measure the droplet's composition with mass spectrometry (MS) (Birdsall et al., 2018). Other single levitated particle MS methods have been reported (Jacobs et al., 2017). Other groups have developed methods to measure vapor pressures of organic compounds using highly precise particle diameter measurements using optical sizing techniques (Krieger et al., 2012). One difference between MS and optical sizing approaches is with MS, vapor pressures of individual chemical components can be readily extracted in a multicomponent system. In this research article, we report experiments in which we used our EDB-MS instrumentation to measure $P_{\mathrm{vap,eff}}$ of butenedial under different experimental conditions, by measuring butenedial's evaporation rate and fitting the data to a kinetic model in which $P_{\mathrm{vap,eff}}$ is the free parameter. $K_{\mathrm{H,eff}}$ can also be calculated based on a calculated particle water content, using measured relative humidity and a thermodynamic model. First we measured $P_{\mathrm{vap,eff}}$ of butenedial in purely organic aerosol particles under two relative humidity conditions. We then measured $P_{\mathrm{vap,eff}}$ of butenedial in mixed organic/inorganic aerosol particles, containing either sodium chloride or sodium sulfate under humid conditions. The results demonstrate the possible role of different factors on the effective vapor pressures and Henry's law constants of organic aerosol components, as well as help inform future EDB-MS experiments.

2 Experimental

2.1 Butenedial synthesis

Butenedial was synthesized in our laboratory following literature procedure (Avenati and Vogel, 1982). In brief, 2.4 M 2,5-dihydro-2,5-dimethoxyfuran (DMDF, TCI America, 98%) was hydrolyzed at 25° C over ~10 d in aqueous solution containing acetic acid (VWR, 99.7%) diluted to 3.4 M in deionized water. Reaction progress was monitored via NMR. Rotary evaporation was used to remove acetic acid, residual DMDF, and excess water. The mass fraction of the rotovapped solution determined to be butenedial was quantified via quantitative addition of diethylmalonic acid (Sigma Aldrich, 98%) as an internal standard, and found to be 0.75±0.02, with the lack of major unidentified peaks in the spectrum implying the balance of the composition to consist of water. No further purification was deemed necessary based on the collected product NMR spectrum (Fig. 3).

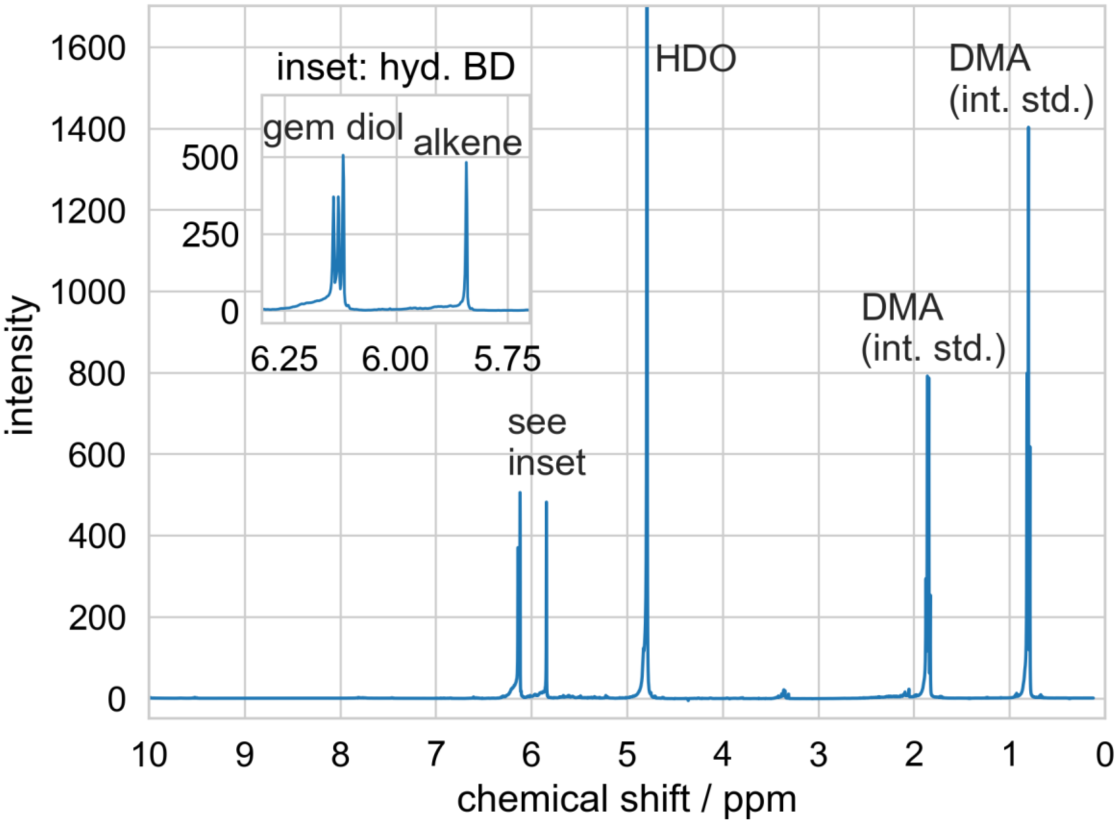

Figure 3: NMR spectrum of synthesized butenedial in deuterated water solvent. Includes peaks associated with hydrated butenedial (hyd. BD), diethylmalonic acid (DMA), used as an internal standard (int. std.), and solvent (HDO).

2.2 Droplet levitation and measurement

Microdroplets were generated, levitated, and measured via mass spectrometry using the same electrodynamic balance–mass spectrometry (EDB-MS) apparatus as previously described (Birdsall et al., 2018). In brief, a droplet-on-demand particle generator injects a ~140 pL droplet from an aqueous solution into the EDB levitation chamber, through a charged coil that gives the droplet charge. A combination of AC and DC electrodes, in a “dual-ring” geometry, establishes an electric field that confines the charged droplet in the center of the levitation chamber. The water content from the aqueous solution rapidly equilibrates with the relative humidity of the levitation chamber (~1 s). A single droplet is allowed to reside in the center of the levitation chamber for a defined period of time while a purge flow of dry or humidified nitrogen gas flows through the levitation chamber (95 standard cubic centimeters per minute, sccm), maintaining a fixed relative humidity (RH) in the levitation chamber and preventing the accumulation of gases evaporating from the droplet. At the end of the residence time in the droplet levitation chamber, the gas flow and electric field are manipulated to eject the droplet out of the bottom of the levitation chamber, through a straight length of 1/4" (outer diameter) stainless steel tubing to the ionization region. In the ionization region, which like the levitation chamber is at ambient pressure, the droplet impacts a glass slide mounted on a heated plate (220° C) and the resulting vapors are ionized via a corona discharge emanating from a charged needle and drawn into the inlet of a commercial time-of-flight mass spectrometer, operated at unit mass resolution (JEOL AccuTOF). A sample mass spectrum of a single particle containing butenedial, hexaethylene glycol (PEG-6, an internal standard) and sodium chloride is shown in Fig. 4.

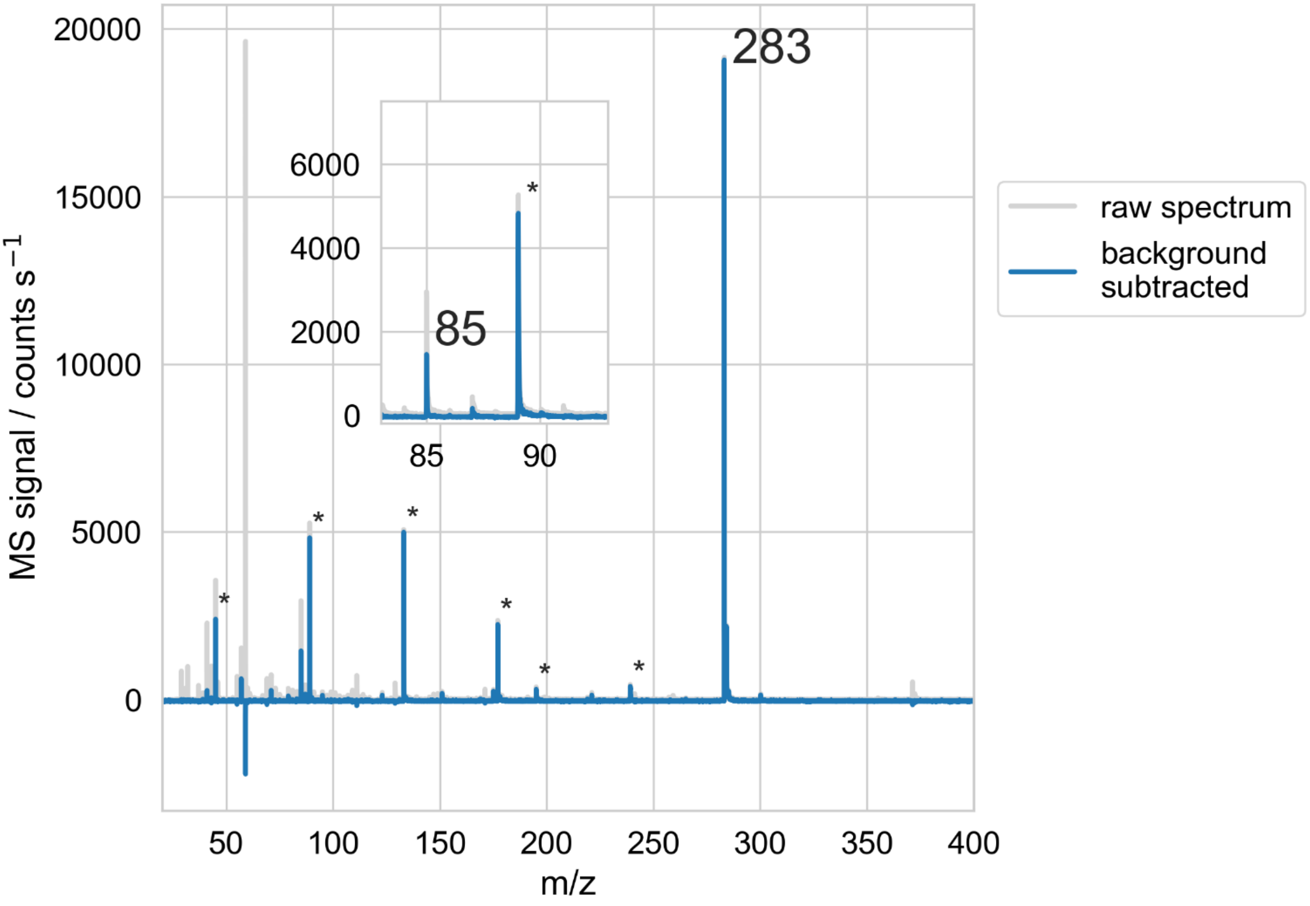

Figure 4: Sample mass spectrum of droplet trapped in EDB and measured with MS, using the BD + PEG-6 + NaCl (X_{NaCl} = 0.140) experimental solution. Both the raw and background-subtracted spectra are shown. Butenedial is observed at its parent ion of 85 m/z. PEG-6 is observed at its parent ion of 283 m/z, along with at known fragment m/z labeled with *.

Mass spectra were collected using commercial software (JEOL MassCenter), resulting in a brief (few second) signal "pulse" above the background on m/z channels corresponding to components of the vaporized droplet (Fig. 5). As previously, the intensity at each m/z channel was quantified as the height of the pulse above the background. The peak height calculation was automated using an algorithm that detected the peak at each mass channel of interest and subtracted an average background value from before the peak onset, and was checked by eye for correctness.

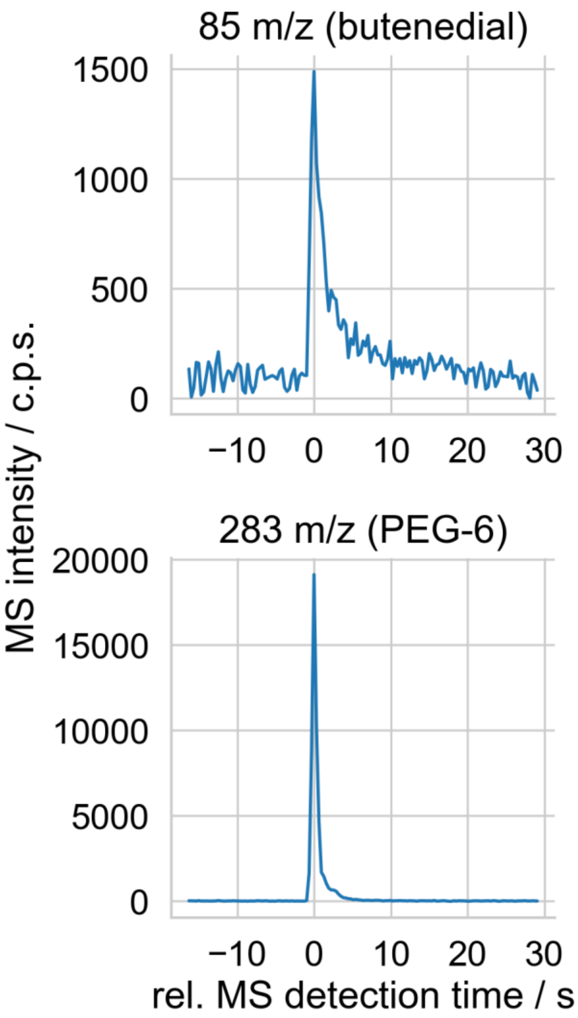

Figure 5: Sample extracted ion time series from measurement of a single droplet, whose mass spectrum is shown in Fig. 4. The peak intensities in the 85 and 283 m/z mass channels above the surrounding background are used to quantify the abundance of butenedial and PEG-6 in the droplet, respectively.

One change from the previously described setup was to sample the mass spectrometer at a faster rate of 3 Hz, compared to previous sampling at 1 Hz. Each mass spectrum had sufficient signal, with better temporal sampling of the droplet signal peak. With the current set of experiments, we observed less particle-to-particle variability in the normalized analyte signal compared to previously (Birdsall et al., 2018). This could potentially be explained by our previous technique undersampling the peak shape.

As previously described (Birdsall et al., 2018), droplet sizes were characterized after initial trapping and before the ejection procedure using a spring point technique, which relies on a quantitative relationship of the visible onset of droplet instability (the "spring point") in the EDB with the voltage conditions and the droplet diameter (Davis, 1985). The droplet diameters determined for this study used the same calibration data using 18 μm diameter polymethylmethacrylate (PMML) spheres as previously. The absolute accuracy of this technique is estimated at 20%.

2.3 Experimental systems

We used two types of experiments to probe the effect of relative humidity (RH) and inorganic content on evaporation rate of butenedial and on extracted values of $P_{\mathrm{vap,eff}}$ and $K_{\mathrm{H,eff}}$. The experimental solutions used in the current study are reported in Table 1. Overall two types of experiments were performed.

Table 1: Parameters describing the experimental conditions used in each experiment type. These parameters and associated uncertainties were used as model inputs. Relative molar quantities of butenedial, PEG-6 and the inorganic salts were determined via the mass composition of the prepared precursor solution. The overall mole fraction of water was calculated from the experimental relative humidity (75±5% for the humid experiments and 2.5±2.5% for the dry experiments) and the solution composition via the thermodynamic model AIOMFAC (see body text). Radius measurements were obtained via a spring point technique (see body text). Provided uncertainties are 1σ values and incorporated into the model calculations as explained in the main text. *Radius distribution imputed from dry BD + PEG-6, adjusted by factor of 1.12 to account for presence of water. **Radius distribution imputed from NaCl (#1) experiment.

composition	RH	X_{BD}	$X_{\mathrm{PEG-6}}$	X_{NaCl}	$X_{\mathrm{Na_2SO_4}}$	$X_{\mathrm{H_2O}}$	r (μm)	T (K)	N
BD + PEG-6	<5%	0.457 ± 0.013	0.518	0	0	0.025 ± 0.013	12.9 ± 1.5	300.10 ± 0.75	19
BD + PEG-6	75 ± 5%	0.0960 ± 0.0028	0.109	0	0	0.795 ± 0.013	14.4 ± 1.7*	300.10 ± 0.75	9
BD + PEG-6 + NaCl (#1)	75 ± 5%	0.0976 ± 0.0026	0.0514	0.071	0	0.780 ± 0.020	13.8 ± 2.1**	300.10 ± 0.75	16
BD + PEG-6 + NaCl (#2)	75 ± 5%	0.0255 ± 0.0007	0.0145	0.140	0	0.820 ± 0.015	13.8 ± 2.1**	300.10 ± 0.75	17

BD + PEG-6 + Na_2SO_4	75 ± 5%	0.0621 ± 0.0027	0.0528	0	0.105	0.795 ± 0.018	13.8 ± 2.1**	300.10 ± 0.75	8

One type of experiment was designed to investigate the effect of RH on the evaporation rate (and hence $P_{\text{vap,eff}}$) of butenedial. These experiments used droplets from a solution containing a mixture of butenedial and hexaethylene glycol (PEG-6, i.e., the polyethylene glycol hexamer, 99%, Sigma Aldrich), the latter of which served as an internal standard for reasons discussed in Sect. 2.3.1. Droplets were exposed to two different RH levels: "dry" experiments for which the bath gas was dry nitrogen gas with RH in the EDB measured to be <5%, and "humid" experiments for which the bath gas was humidified nitrogen gas created by flowing nitrogen gas through a water bubbler with RH in the EDB measured to be 75 ± 5%.

A second type of experiment was designed to probe the effect of the presence of inorganic species on $P_{\text{vap,eff}}$ of butenedial. As for the RH experiments, droplets contained butenedial along with PEG-6 acting as an internal standard. Additionally the droplets contained one of two inorganic compounds, either sodium chloride (NaCl) or sodium sulfate (Na_2SO_4). Two NaCl solutions were studied with X_{NaCl} of 0.071 and 0.140; one Na_2SO_4 solution was studied with $X_{\text{Na}_2\text{SO}_4}$ of 0.105. These experiments were performed with a humidified levitation chamber at RH 75 ± 5%.

Separate trials in a similarly designed EDB equipped with additional spectroscopic instrumentation (described in Sect. 3.2 of Krieger et al. (2018)) were performed to confirm the particles remained deliquesced at our experimental humidity for the inorganic particles. The observed two-dimensional angular optical scattering pattern remained visible at the experimental humidity, implying a spherical deliquesced particle (Braun and Krieger, 2001). No change in fringe pattern was observed when drying a particle containing butenedial and PEG-6 without an inorganic salt, meaning that no phase separation or efflorescence occurred in the salt-free system. In contrast, when dry nitrogen was introduced as the bath gas for salt-containing particles, the fringe pattern was observed to change, indicating that efflorescence had occurred due to the presence of the inorganic salt.

2.3.1 PEG-6 as internal standard

We deemed PEG-6 to be an appropriate internal standard and major condensed-phase component for these experiments for a number of reasons. PEG-6 was used as an internal standard to account for droplet-to-droplet variability in total amount of signal measured with the mass spectrometer because it shows a clear peak at 283 m/z in the mass spectrum (MH^+) and its vapor pressure is low enough for its evaporation to be negligible over the timescale of the experiments. We also used PEG-6 as an internal standard in a previous set of experiments (Birdsall et al., 2018). Based on those previous results, the viscosity of a PEG-6 matrix is sufficiently low to expect no condensed-phase diffusion effects limiting the evaporation rate of butenedial.

We also verified our observations were not affected by reactive chemistry between PEG-6 and butenedial. Because butenedial contains aldehyde groups and PEG-6 contains alcohol groups, conceivably a hemiacetal could be formed by their reaction, which would lower $P_{\mathrm{vap,eff}}$ of butenedial. We repeated the humid evaporation measurements with diethylmalonic acid as the internal standard rather than PEG-6, for which no chemical reaction with butenedial is expected. We observed no difference in evaporation rate, within experimental uncertainty, of butenedial between the PEG-6 and diethylmalonic acid data, implying the presence of PEG-6 did not measurably influence the evaporation rate. Furthermore, we observed no peaks in the mass spectrum at m/z ratios consistent with a PEG-6–butenedial hemiacetal. Recent work has shown that a model hemiacetal oligomer was detected intact via mass spectrometry when quickly (millisecond timescale) vaporized from impact onto a heated rod at ~160 °C (Claflin and Ziemann, 2019), which suggests under our similar analytical conditions we would also expect to observe the intact hemiacetal, if present. Nor did we observe a peak in a 2D NMR heteronuclear multiple bond correlation (HMBC) experiment of the precursor PEG-6–butenedial aqueous solution consistent with coupling between the butenedial and PEG-6 moieties of a putative hemiacetal, as would be expected.

To check whether salting out of PEG-6 would affect the extracted butenedial $P_{\mathrm{vap,eff}}$ in the inorganic experiments, additional evaporation model runs (see Sect. 2.4) were performed in which the model representation of PEG-6 had a vapor pressure 10 times larger than the literature value. This was used as a conservative upper bound of a salting-out effect. With this higher vapor pressure of PEG-6, evaporation of PEG-6 still proceeded slowly enough over experimental timescales such that there was no discernible difference in the extracted butenedial $P_{\mathrm{vap,eff}}$ (<1% change).

2.4 Evaporation model and determination of $P_{\mathrm{vap,eff}}$ and $K_{\mathrm{H,eff}}$

$P_{\mathrm{vap,eff}}$ of butenedial under each experimental condition was determined by fitting a kinetic model that describes the changing composition of a droplet in time to observations. To determine the uncertainty in the extracted $P_{\mathrm{vap,eff}}$, the analysis considered the uncertainty in the model input parameters and the ~~standard error~~uncertainty introduced by shot-to-shot noise in ~~the non-linear curve fitting coefficient~~collected data, as detailed below. The data consists of a set of individual observations for each trapped and measured droplet, corresponding to a normalized abundance of remaining butenedial (relative to PEG-6) after butenedial evaporation has proceeded for a certain amount of time. Plotting a set of these data points for a single type of experiments shows a decay over time in the normalized butenedial signal~~, which is~~. The individual data points are binned by time spent in the EDB, and bootstrapped realizations of the binned data are compared to the kinetic model.

2.4.1 Maxwell flux description of particle evaporation

The kinetic model describing evaporation was implemented in pyvap, an open-source Python package that has been previously described (Birdsall et al., 2018). In brief, the kinetic model numerically integrates a differential equation describing evaporation of droplet components via Maxwellian flux (Seinfeld and Pandis, 2006), as in Eq. 1:

$$\frac{dn_i}{dt} = 4\pi r D_{\mathrm{g}_i}(c_{\infty_i} - c_{\mathrm{s}_i}) \qquad (1)$$

in which r is the particle radius, D_{g_i} is the gas-phase diffusion constant of species i, and c_{∞_i} is the gas-phase concentration of species i at infinite distance from the particle surface (taken to be zero in the EDB), and c_{s_i} the gas-phase surface concentration of species i. We assume the particle is an ideal mixture and in equilibrium at its surface with the gas phase, so the gas-phase surface concentration is then given by Eq. 2:

$$c_{s_i} = X_i \frac{P_{\mathrm{vap}_i,\mathrm{eff}}}{kT} \qquad (2)$$

where X_i is the particle-phase mole fraction of species i, $P_{\mathrm{vap}_i,\mathrm{eff}}$ is the pure component vapor pressure of species i at temperature T inside the EDB, and k is the Boltzmann constant. Because the droplet surface is curved, the vapor pressure of a compound above a charged levitated droplet could conceivably be elevated due to the Kelvin effect. The particle charge also could lower the vapor pressure of a compound with a significant dipole moment. However, following Sect. C1 of Huisman et al. (2013) to calculate the combined Kelvin and charge stabilization effects, we conclude the effects are negligible considering the particle diameter and charge for these experiments.

Due to the fast equilibration of water, its evaporation is not explicitly represented. Instead, the water content is calculated at each time step to preserve a fixed mole fraction of water in the particle. The evaporation of PEG-6 is explicitly represented using experimental physical parameters available in a review of polyethylene glycol vapor pressures (Krieger et al., 2018). However, over the experimental timescales involved the evaporation of PEG-6 was calculated to be negligible, making for our purposes PEG-6 effectively involatile. The model representations of sodium chloride and sodium sulfate had vapor pressures of 0, preventing any modeled evaporation. Sodium chloride and sodium sulfate are represented as being fully dissociated into two and three ions, respectively. The model does not include any representation of acid-base equilibrium.

To make the fitting procedure less computationally expensive, rather than repeatedly numerically integrating the differential equation we developed an analytical expression that approximates a solution to Maxwellian flux under certain simplifying assumptions. In particular, we assumed droplet radius and mole fraction of water were time-invariant, and all non-butenedial, non-water droplet components did not evaporate over the experimental time scale. A description of the resulting analytical solution and fitting procedure, along with validation of the technique, are given in Sect. S1 and S2.

2.4.2 Parameter inputs and uncertainty

All parameters aside from $P_{\mathrm{vap,eff}}$ of butenedial are constrained by knowledge of the experimental system. These parameters include the initial mole fraction of butenedial, temperature, RH, the gas-phase diffusivity of butenedial, and the initial droplet radius. The droplet diameter is provided by the spring-point measurements. The temperature and RH is provided by a RH/temperature probe (Sensirion SHT31).

Physical parameters used to represent each compound are given in Table 2. Other model input parameters are given in Table 1.

Table 2: Physical parameters for each compound used in the model. *Note that because all observations of butenedial in the condensed phase were consistent with existing in its dihydrated form, the model used physical parameters of butenedial dihydrate. **Because inorganic salts sodium chloride and sodium sulfate are essentially involatile, their vapor pressures were assumed to be effectively 0.

compound	M (kg / mol)	ρ (kg / m³)	$P(298\mathrm{K})$ (Pa)	D_{gas} (10^{-6} m^2 / s)
butenedial dihydrate	0.1201*	1060	see results	8.56 ± 0.86
PEG-6	0.2823	1180	3.05×10^{-5}	4.26
NaCl	0.05844	2160	0**	n/a
Na_2SO_4	0.142	2660	0**	n/a

The gas-phase diffusivity of butenedial (along with the dihydrate) in air was estimated using the Fuller-Schettler-Giddings equation, which is based on the molecular weights and volumes of the components of a binary gas mixture. The molecular volume of butenedial was calculated based on its molecular structure using literature parameters (Welty et al., 1984). The density of butenedial is assumed to be 1.06 g m^{-3} based on literature densities of aldehydes butanedial and glutaraldehyde (Lide, 2008).

The initial molar ratio of butenedial and other non-water components of the droplet (e.g., PEG-6, sodium chloride, sodium sulfate) is known from the relative concentrations of the compounds in the precursor aqueous solution, which was prepared quantitatively. However, the overall mole fraction of butenedial in the droplet depends on the droplet's water content. For the dry experiment the RH is measured to be 5% or lower. Though the possible presence of water in these low amounts are accounted for in our uncertainty analysis (see below), we find under these conditions the presence of water has a negligible effect on accurately predicting the mole fraction of butenedial. In contrast for the humid experiments the water content is a non-negligible contribution to the overall molar composition. When equilibrated with the surrounding gas phase, the droplet water concentration will be such that the activity of water in solution and in the gas phase (i.e., RH) are equal.

To calculate the mole fraction of water corresponding to the RH of the humid experiments we used the thermodynamic model AIOMFAC via its publicly accessible online interface (https://aiomfac.lab.mcgill.ca), using the known starting composition of the non-water particle components. AIOMFAC uses a functional group approach to calculate the equilibrium thermodynamic activities of a mixed inorganic/organic solution assumed to exist in a single deliquesced phase (Zuend et al., 2011, 2008). In particular, butenedial was defined in terms of its functional groups in its hydrated form because our results imply that is its dominant form in our experiments (see below). The mole fraction of water in the particle, $X_{\mathrm{H_2O}}$, was assumed to be fixed over the entire course of the experiment, ~~assuming~~which is true if the activity coefficient of water does not change appreciably as butenedial evaporates from the particle. We checked the validity of the assumption by using AIOMFAC to compare the change in calculated $X_{\mathrm{H_2O}}$ for the humid, inorganic-free experiment, between its initial composition and composition after all butenedial evaporated. We found the change in calculated $X_{\mathrm{H_2O}}$ to be approximately 0.005, implying the effect of this assumption on our results is negligible within other sources of uncertainty.

Because of the different molar sensitivities of the mass spectrometer to butenedial and PEG-6, a scaling factor needed to be applied to scale the measured ratios of butenedial and PEG-6 signal intensities to the molar ratio. The scaling factor was determined independently for each type of experiment from the data points for the droplets that had resided in the EDB for 5 minutes or less. Assuming negligible butenedial evaporation over this timescale, the molar ratio for these droplets was assumed to be equal to the known starting molar ratio of the precursor aqueous solutions. A bootstrapping procedure was used to estimate the mean and standard deviation in the short time interval normalized peak intensity, and from that along with the known molar composition of the starting precursor aqueous solution, a mean and standard deviation in the scaling factor was determined.

Spring-point-derived radii were available for the dry experiment (16 radii, mean 12.9 µm and standard deviation 1.5 µm) and NaCl #1 experiment (16 radii, mean 13.8 µm and standard deviation 2.1 µm). Spring-point-derived sizes were not available for the humid (inorganic-free), NaCl #2, and Na_2SO_4 experiments. However, due to the similarity in droplet behavior (e.g., response to flow and voltage conditions during particle transfer) the distribution of droplet diameters for those experiments could be imputed from the available measurements. The humid experiment diameter distribution was obtained by scaling the dry experiment diameter distribution by a factor of 1.115 to account for the calculated increase in diameter due to the presence of water. The NaCl #2 and Na_2SO_4 experiment diameter distributions were assumed to match that of the NaCl #1 experiment. The resulting diameter distributions used are given in Table 1.

We used a combined Monte Carlo and bootstrapping approach to estimate the uncertainty in the retrieved butenedial $P_{\mathrm{vap,eff}}$ due to uncertainties in the other model input parameters. The implementation of the uncertainty analysis is described in Sect. S3. The analysis incorporates the uncertainty associated with model input parameters, including droplet diameter, temperature, scaling factor, and gas-phase diffusivity of butenedial, as reported in Table 1. Using this approach, the per-experiment uncertainties due to uncertainty in model input parameters and ~~standard error~~shot-to-shot noise in the ~~model fit~~data vary by experiment and are reported in Table 3~~, but range between ±20% and ±40%.~~ as 95% confidence intervals. Compared to other uncertainties in our approach, this is likely a dominant source of uncertainty. For comparison, we previously described an uncertainty estimation technique in which we simply considered limiting cases of temperature and diameter parameters to give upper and lower bounds of $P_{\mathrm{vap,eff}}$ of various polyethylene glycols (Birdsall et al., 2018). Using that less detailed uncertainty treatment, which did not consider uncertainty due to measurement variability, the previous estimated uncertainty range was between ±15% and ±25%.

Table 3: Extracted effective vapor pressures $P_{\mathrm{vap,eff}}$ for butenedial (BD) with ~~1σ uncertainties~~95% confidence interval bounds (given within parentheses) obtained from uncertainties in model input parameters described in the main text, along with effective Henry's law constants $K_{\mathrm{H,eff}}$ and Setschenow constants K_{S}, where applicable. Uncertainties in $K_{\mathrm{H,eff}}$ and K_{S} derived from propagating uncertainties in associated $P_{\mathrm{vap,eff}}$ values.

composition	RH	ionic strength (M)	$P_{\mathrm{vap,eff}}(BD, 300K)$ (mPa)	$K_{\mathrm{H,eff}}$ (10^7 M atm^{-1})	K_{S} (m^{-1})
BD + PEG-6	<5%	n/a	~~31~~28.1 ~~± 9.0~~(13.1, 47.8)	n/a	n/a
BD + PEG-6	75 ± 5%	n/a	~~39.5 ± 8.6~~34.2 (18.8, 54.9)	~~5.2 ± 1.1~~6.0 (3.7, 11)	n/a
BD + PEG-6 + NaCl (#1)	75 ± 5%	5.3	~~58 ± 18~~66 (36, 105)	~~4.8 ±~~ 3.1~~.~~ (2.0, 5.7)	+0.~~009 ±~~ 056 (0.~~032~~012, 0.16)
BD + PEG-6 + NaCl (#2)	75 ± 5%	9.6	~~224 ± 89~~169 (71, 301)	1.~~82 ±~~ 2 (0.~~71~~68, 2.9)	+0.~~048 ±~~ 074 (0.~~021~~047, 0.15)
BD + PEG-6 + Na_2SO_4	75 ± 5%	21.0	~~172 ± 44~~177 (64, 376)	1.~~54 ±~~ 2 (0.~~40~~55, 3.2)	+0.~~073 ±~~ 096 (0.~~020~~056, 0.21)

2.4.3 Effective Henry's law constant

Using the extracted $P_{\mathrm{vap,eff}}$ along with the calculated molarity of butenedial, we estimated an effective Henry's law constant $K_{\mathrm{H,eff}}$ for all humid experiments. The butenedial molarity was calculated using the water content calculated with the thermodynamic model AIOMFAC (Section 2.4.2) and assuming the overall molecular weight and density of the particle was the weighted average of the molecular weights and densities of its chemical components, respectively. The full expression is then given by Eq. 3:

$$K_{\mathrm{H,eff}} = \frac{X_{\mathrm{BD}} MW_{\mathrm{avg}}^{-1} \rho_{\mathrm{avg}}}{X_{\mathrm{BD}} P_{\mathrm{vap,eff}}} \qquad (3)$$

or after simplification

$$K_{H,eff} = \frac{MW_{\mathrm{avg}}^{-1}\rho_{\mathrm{avg}}}{P_{\mathrm{vap,eff}}} \qquad (4)$$

where MW_{avg} is the weighted average of molecular weights of the chemical components of the particle and ρ_{avg} is the weighted average of densities of the chemical components of the particle.

Because the dominant source of uncertainty in Eq. 4 is $P_{\mathrm{vap,eff}}$, we derive the ~~uncertainty~~95% confidence interval in $K_{\mathrm{H,eff}}$ by using the same ~~relative uncertainty~~95% confidence interval as in the corresponding $P_{\mathrm{vap,eff}}$.

3 Results and discussion

3.1 Humidity dependence

Figure 6 shows data and the corresponding best model fit for the humidity dependence butenedial evaporation experiments. The extracted values for the extracted $P_{\mathrm{vap,eff}}$ of butenedial under the two RH conditions are ~~31~~28.1 ~~± 9.0~~ mPa (95% CI 13.1 mPa, 47.8 mPa) and ~~39.5 ± 8.6 mPa~~34.2 mPa (95% CI 18.8 mPa, 54.9 mPa) for the dry and humid conditions, respectively. (The uncertainty values correspond to a ~~1σ value~~95% confidence interval derived from the combined Monte Carlo sampling and bootstrapping approach described in the SI, and reflects the uncertainty due to uncertainty in the model input parameters and the ~~standard error of the coefficient~~shot-to-shot noise in the ~~model fit~~data.) We interpret these results to imply $P_{\mathrm{vap,eff}}$ under the dry and humid conditions are indistinguishable, within the uncertainties in our measurements and fitting procedure. Note the extracted $P_{\mathrm{vap,eff}}$ values are similar despite the differences in evaporation timescales. This is a consequence of the evaporation rate scaling with the concentration of butenedial in the particle in Eq. 2. Because the mole fraction of butenedial decreases as water content increases, under humid conditions butenedial evaporation is expected to proceed more slowly even if $P_{\mathrm{vap,eff}}$ is unchanged. This previously has been referred to as the "Raoult's Law effect" (Prisle et al., 2010).

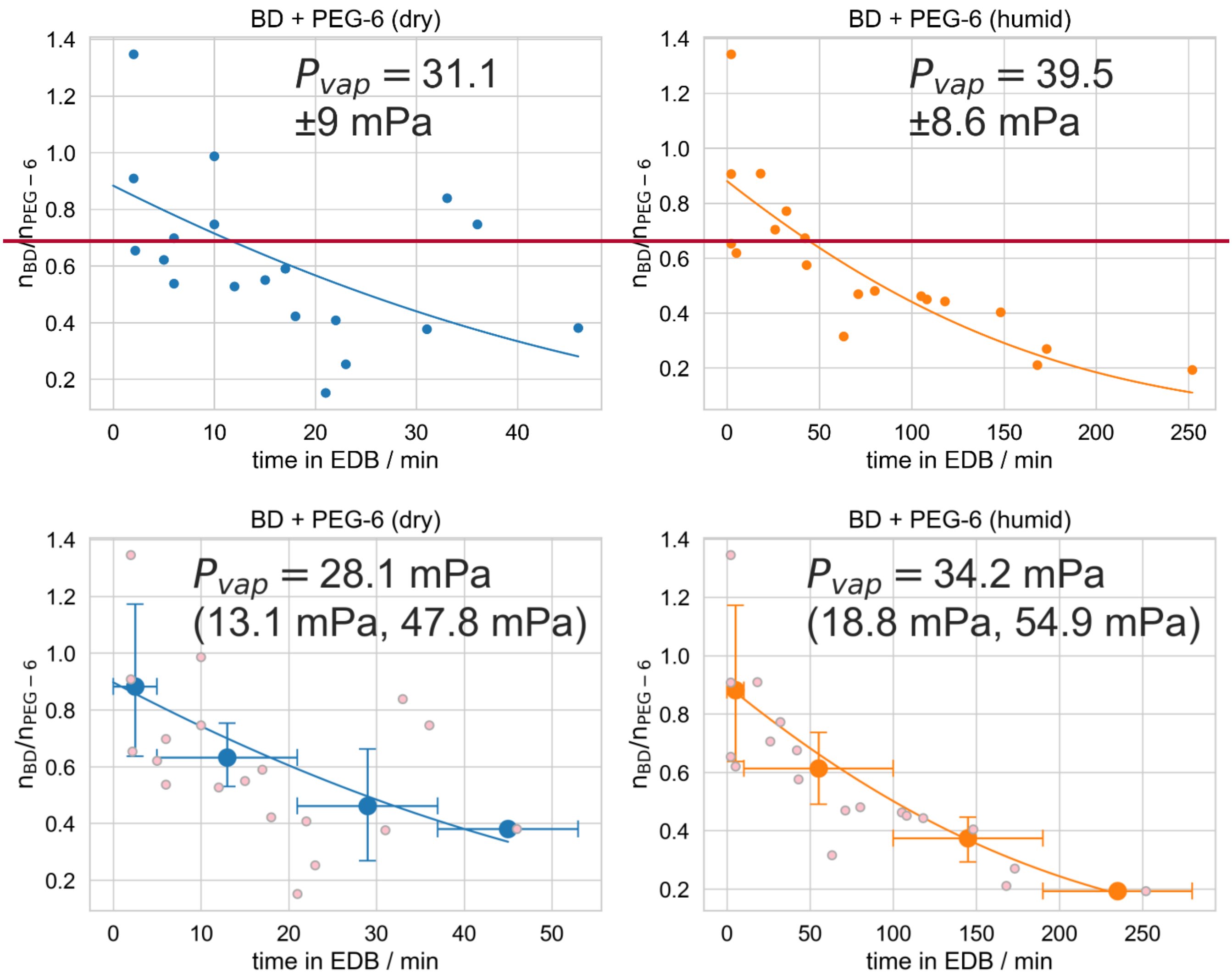

Figure 6: Experiments used to determine the effective vapor pressure of butenedial (BD) in a droplet also containing hexaethylene glycol (PEG-6), under dry (RH<5%) and humid (RH 75 ± 5%) conditions. ~~Points~~Small pink points are observations of individual droplets and the line is the best model fit, as described in the text. Large points are the mean binned values from the bootstrapping procedure, with ~~associated~~x error bars showing the width of the bins and y error bars representing a 95% confidence interval of the mean value in the bin, over all bootstrapped realizations. The plotted model fit is for the mean vapor pressure ~~and 1σ uncertainty printed~~obtained by averaging over all model fits to all realizations. The vapor pressure is reported as a 95% confidence interval over repeating the fitting procedure over 10000 bootstrapped realizations.

One implication of the measured effective vapor pressures is that considering the hydration of butenedial is crucial for a correct prediction of its $P_{\text{vap,eff}}$ and hence its gas–particle partitioning behavior. If the butenedial in the particle primarily consisted of butenedial in its dialdehyde form, the expected $P_{\text{vap,eff}}$ would be expected to be orders of magnitude larger. For example, the EVAPORATION model (Compernolle et al., 2011) (accessed through UManSysProp (Topping et al., 2016)) predicts a vapor pressure for butenedial of 350 Pa at 298 K, and the Nannoolal et al. method (Nannoolal et al., 2008) (also accessed through UManSysProp) predicts an even higher vapor pressure of 1.5 kPa at 298 K. If butenedial were primarily in the form of the dialdehyde, we would expect to observe a much faster rate of evaporation than was actually observed. In contrast, using the dihydrated form of butenedial, EVAPORATION predicts a vapor pressure of 2.2 mPa at 298 K, which is almost within the same order of magnitude as the measured butenedial $P_{\text{vap,eff}}$. The Nannoolal et al. method predicts a very low vapor pressure of 2.5 x 10^{-4} mPa at 298 K for the butenedial dihydrate.

Both EVAPORATION and the Nannoolal et al. method use a group contribution approach; the extremely low value of the Nannoolal et al. method prediction may reflect the limitations of its group contribution parameterization for this chemical structure. Additionally, in comparison with experimental vapor pressures, EVAPORATION has been reported to show a trend of underestimating vapor pressures at low vapor pressure (O'Meara et al., 2014). This trend could help account for the discrepancy between our measured $P_{\text{vap,eff}}$ and the EVAPORATION model estimate, though we cannot rule out the possibility that the discrepancy between measured $P_{\text{vap,eff}}$ and predicted butenedial dihydrate vapor pressure could possibly reflect a contribution to $P_{\text{vap,eff}}$ by the evaporation of butenedial monohydrate present in the particle. EVAPORATION predicts the monohydrate to have a vapor pressure of 2.3 Pa, whereas the Nannoolal et al. 2008 method predicts a vapor pressure of 220 mPa. However, the lack of any significant aldehyde peak in the NMR spectrum suggests equilibrium strongly favors the dihydrate form of butenedial under humid conditions.

The low observed $P_{\text{vap,eff}}$ of butenedial conceivably could also reflect a contribution from formation of butenedial oligomers, which would similarly lead to a lower $P_{\text{vap,eff}}$. However, we see no evidence for oligomer formation in our mass spectra or NMR spectrum. For oligomer formation to be consistent with our observations, it would have to be the case that ether oligomers hypothetically formed from butenedial completely decompose or fragment during the vaporization and ionization process into butenedial monomers that are detected at the butenedial ion parent ion value of 85 m/z. The likelihood of complete oligomer decomposition appears low. A recent study of different classes of model oligomers reported ether oligomers were detected intact via mass spectrometry after thermal desorption at ~160 °C (Claflin and Ziemann, 2019). Because we have no observational evidence for oligomer formation, in contrast to our observation of extensive butenedial hydration in NMR spectra, we conclude hydration of butenedial is the more likely explanation for the observation of a relatively low $P_{\text{vap,eff}}$. Finally, as elucidated in Sect. 2.3.1, we observe no evidence for formation of cross-products of butenedial reacting with PEG-6 that would reduce the $P_{\text{vap,eff}}$ of butenedial.

Furthermore the fact that the two $P_{\text{vap,eff}}$ are indistinguishable, at least within the estimated uncertainty ~~of ~30%,~~, implies butenedial primarily exists in a hydrated form not only under conditions with a high water content, but also under conditions with lower water content. This observation is also consistent with the collected NMR spectra of butenedial, in which only hydrated butenedial peaks are observed, even under conditions with a lower residual water content. There may be to some degree a shift in equilibrium between the hydrated and non-hydrated forms of butenedial under the different RH conditions, which could lead to a change in $P_{\text{vap,eff}}$, but our results imply any change would correspond to a change in $P_{\text{vap,eff}}$ less than our uncertainty in extracted $P_{\text{vap,eff}}$~~, approximately 20%.~~.

A possible mechanistic explanation for this observation could be due to slow kinetics of dehydration under dry conditions. For all experiments, regardless of RH, the particle was initially generated from an aqueous solution in which equilibrium appears to strongly favor butenedial dihydrate. When the droplet is injected into the EDB under dry conditions, the water content of the particle quickly (~1 s) equilibrates. Within the dry particle, butenedial may be kinetically frozen over experimental timescales in the dihydrate form, even if the dialdehyde becomes more thermodynamically favorable. Additional experiments would be necessary to test this explanation.

Using Eq. 4 we calculated $K_{\text{H,eff}}$ of butenedial to be ~~5.2 ± 1.1~~6.0 (95% CI 3.7, 11) × 10^{7} M atm^{-1} in the humid, inorganic-free experiment. (Uncertainties in $K_{\text{H,eff}}$ arise from propagating uncertainties in $P_{\text{vap,eff}}$, given the relationship in Eq. 4.) For comparison, $K_{\text{H,eff}}$ of glyoxal has been previously measured to be 4.19 × 10^{5} M atm^{-1} in an inorganic-free aqueous phase (Ip et al., 2009). The magnitude of the measured $K_{\text{H,eff}}$ for butenedial compared to glyoxal suggests butenedial may have a strong tendency to partition into an available aqueous phase, ignoring the effect of inorganic compounds.

3.2 Inorganic salt dependence

Figure 7 shows data for inorganic salt dependence experiments. For both the sodium chloride and sodium sulfate experiments, the extracted butenedial $P_{\text{vap,eff}}$ is larger than the $P_{\text{vap,eff}}$ measured in the organic-only cases, with values of ~~58 ± 18~~66 mPa ~~and 224 ± 89~~(95% CI 36 mPa, 105 mPa) and 169 mPa (95% CI 71 mPa, 301 mPa) for the X_{NaCl} of 0.071 and 0.140 sodium chloride experiments, respectively, and ~~172 ± 44~~177 mPa (95% CI 64 mPa, 376 mPa) for the sodium sulfate experiment. The fact that the $P_{\text{vap,eff}}$ for butenedial becomes higher in solutions containing both inorganic salts, by up to a factor of ~~8~~5 under our experimental conditions, implies the inorganic salts in this case have a salting-out effect. Interestingly, previous work with a different dialdehyde, glyoxal, demonstrated that the presence of both sodium chloride and sodium sulfate led to a shift in the hydration equilibrium favoring the formation of the hydrate, implying a salting-in effect (Waxman et al., 2015; Yu et al., 2011). In contrast, the three-carbon dicarbonyl methylglyoxal has been measured to exhibit a salting-out effect for both sodium chloride and sodium sulfate (Waxman et al., 2015). The fact that salting-out effects have now been observed for both methylglyoxal and butenedial suggests the direction of salting in/salting out for a dicarbonyl compound may be influenced by the extent to which it contains hydrophobic regions, represented in butenedial by the alkenyl group and in methylglyoxal by the methyl group.

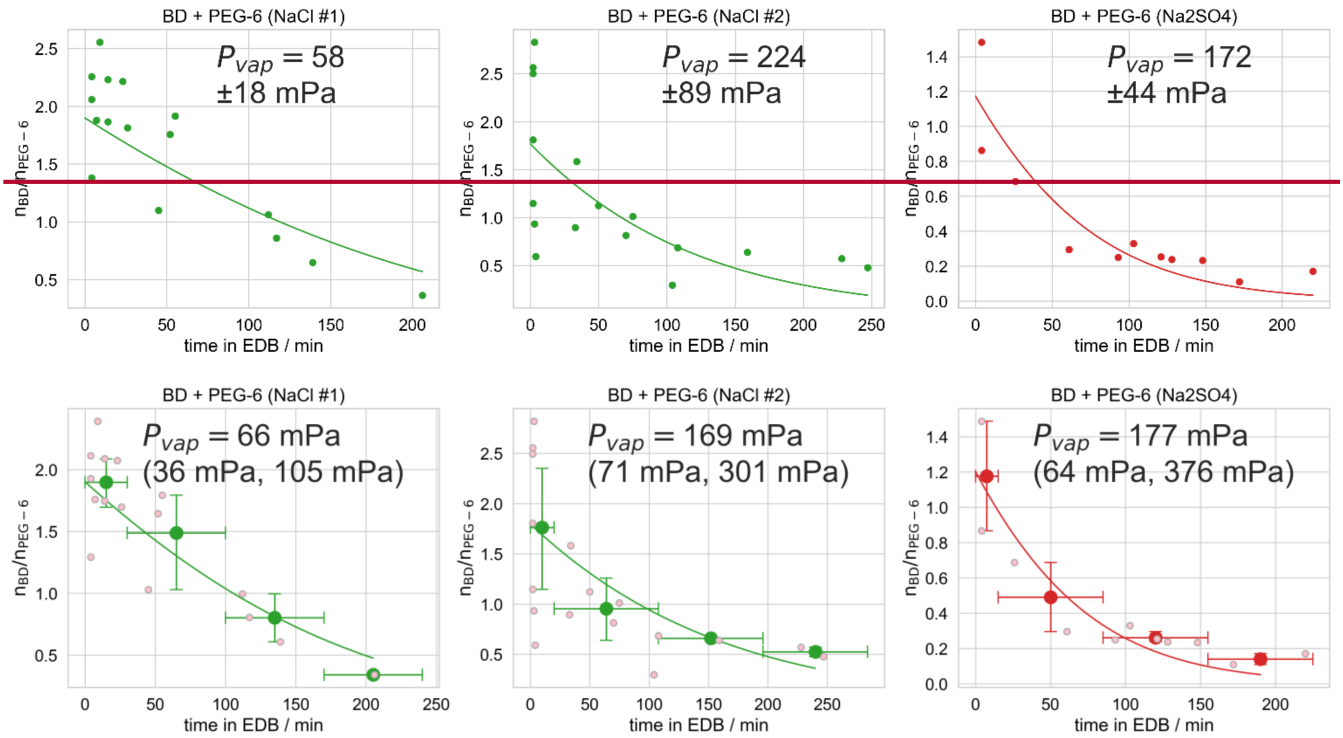

Figure 7: Experiments used to determine the effective vapor pressure of butenedial (BD) in a droplet also containing hexaethylene glycol (PEG-6) and either sodium chloride (NaCl) or sodium sulfate (Na_2SO_4), under humid (RH 75 ± 5%) conditions. ~~Points~~Small pink points are observations of individual droplets and the line is the best model fit, as described in the text. Large points are the mean binned values from the bootstrapping procedure, with ~~associated~~x error bars showing the width of the bins and y error bars representing a 95% confidence interval of the mean value in the bin, over all bootstrapped realizations. The plotted model fit is for the mean vapor pressure ~~and 1σ uncertainty printed~~obtained by averaging over all model fits to all realizations. The vapor pressure is reported as a 95% confidence interval over repeating the fitting procedure over 10000 bootstrapped realizations.

Calculated $K_{\mathrm{H,eff}}$ for the three inorganic salt-containing experiments, again using Eq. 4, are given in Table 3. Furthermore the magnitude of the salting-out effect can be quantified using the Setschenow coefficient K_{S}, using the formulation of Waxman et al. (2015) in Eq. 5, where

$$K_{\mathrm{S}} = \frac{1}{c_{\mathrm{s}} \log \frac{K_{\mathrm{H,w}}}{K_{\mathrm{H,s}}}} \qquad (5)$$

and c_s is the condensed-phase salt concentration (using molality, m), $K_{H,w}$ is the effective Henry's law constant in the absence of the inorganic salt, and $K_{H,s}$ is the effective Henry's law constant in the presence of the inorganic salt. The calculated values of K_S using Eq. 5 for the three inorganic experiments are given in Table 3, with uncertainties derived from propagating the uncertainties in the effective Henry's law constants. The K_S values for the two NaCl experiments (+0.~~009 ±~~056 (95% CI 0.~~032, +~~012, 0.~~048 ± ~~16), +0.~~021 m^{-1})~~074 (95% CI 0.047, 0.15)) have ~~1σ uncertainty intervals that overlap.~~similar values within our uncertainties. K_S for sodium sulfate (+0.~~073 ±~~096 (95% CI 0.~~020 m^{-1})~~056, 0.21)) is ~~approximately three times~~somewhat larger than the ~~mean~~ K_S ~~(+0.029 ± 0.019 m^{-1})~~ for sodium chloride in our experiments~~.~~, though the 95% confidence intervals largely overlap. Interestingly, this is a similar trend as previously reported for methylglyoxal in the presence of the same two inorganic salts, of 0.06 m^{-1} and 0.16 m^{-1}, respectively (Waxman et al., 2015). ~~However, the absolute magnitudes of the K_S values are measured here to be smaller for butenedial compared to methylglyoxal. This may be due to butenedial having two aldehyde groups that are able to hydrate and have relatively energetically favorable interactions with the inorganic salts, compared to only one aldehyde group for methylglyoxal.~~

A competing hypothesis to potentially explain the measured higher $P_{vap,eff}$ in the mixed organic–inorganic droplets could be phase separation. If the presence of the inorganic components led to the formation of two different condensed phases with butenedial predominantly in an organic-rich phase, the $P_{vap,eff}$ of butenedial would be higher due to its higher mole fraction concentration. However, thermodynamic calculations performed in AIOMFAC suggest this behavior is unlikely. Though a more extensive set of calculations would be necessary to rigorously check for the presence of partial phase separation, calculations performed using AIOMFAC assuming a single well-mixed phase under the experimental conditions show the activities of the organic components remain well below 1 without extremely large (i.e., >>1) activity coefficients. These calculations are consistent with the droplets consisting of a single mixed phase under these experimental conditions.

3.3 Sources of uncertainty

The dominant source of uncertainty in our $P_{vap,eff}$ extraction procedure is uncertainty in the droplet diameter. The uncertainty in the measured diameter for a population of particles is estimated to be up to a factor of 50% about the mean, which has a particularly large effect because vapor pressure scales with surface area. Using the spring point technique to measure the starting diameter of each trapped droplet has an inherent uncertainty. Additionally there is some degree in droplet-to-droplet variability in starting diameter for each population of droplets. Our modeling approach treats the diameter of a population of droplets for a single experiment type as a single mean value, with an associated standard deviation. In part we treated the data this way because spring point-derived droplet diameters were not available for every droplet included in this analysis, though consistency in collected data across the data set implied each set of droplets could be described in terms of a single distribution of diameters. Additionally, previous analysis of a data set using spring point diameter measurements did not observe a correlation between residuals of the remaining analyte and the measured starting diameter for that particle, relative to the population mean (i.e., droplets measured using the spring point technique to be smaller than average did not have their analyte molecule evaporate more quickly) (Birdsall et al., 2018). This suggests though there is considerable uncertainty in our spring point measurements, it would not be helpful to constrain the model based on the measured diameter of each individual droplet.

As a secondary effect, uncertainty in water content of the droplets as a calculated parameter may also contribute uncertainty to our $P_{\mathrm{vap,eff}}$ determination. Our representation of the uncertainty in the mole fraction of water reflects solely uncertainty in the relative humidity measurements upon which the model representation is based; we do not include a representation of the accuracy of the AIOMFAC model calculation used to determine the corresponding mole fraction of water itself. The water content is not used to constrain the droplet diameter (which is constrained by the spring point method, above), but it does have a significant effect on determining the overall mole fraction of butenedial in the droplet. For example, the mean measured RH for the humid experiments was 75%, but based on AIOMFAC model calculations the mean mole fraction of water can be up to 0.82, depending on the hygroscopicity of the solution. Because the butenedial is a fixed mole fraction of the non-water portion of the solution, for the same set of measurements a difference in assumed mole fraction of water between 0.75 and 0.82 corresponds to a difference in extracted butenedial $P_{\mathrm{vap,eff}}$ by a factor of (0.18-0.25)/0.25, or almost 30%. Because the true uncertainty in the AIOMFAC activity correction is likely smaller than the difference between the ideal and calculated nonideal cases, 30% likely represents a highly conservative upper bound on uncertainty arising from the AIOMFAC water mole fraction calculation.

4 Conclusions

A set of laboratory experiments have used an electrodynamic balance–mass spectrometry (EDB-MS) technique to measure the evaporation of butenedial from organic-only and mixed organic–inorganic levitated droplets under dry and humid conditions. With this setup the specific process of interest, gas–particle partitioning, was studied in isolation in an environment in which a single particle of known composition is exposed to a continually refreshed bath gas of pure dry or humidified nitrogen. This approach simplifies the measurement compared to performing an experiment in an environmental chamber, which will have a more complex gas-phase matrix, because no gas-phase measurement is required and no process other than evaporation needs to be modeled.

We measured the effective vapor pressure ($P_{\mathrm{vap,eff}}$) of butenedial, under both low (RH<5%) and higher (RH 70%) humidity conditions, to be approximately 30~~-40~~ mPa, which is 4 orders of magnitude lower than the expected vapor pressure of a four-carbon dialdehyde. This result implies butenedial exists primarily in a hydrated form, across a wide range of RH conditions, and the gas–particle partitioning of butenedial in ambient particles favors the particle phase more strongly due to butenedial's hydration. The importance of hydration reactions in affecting gas–particle partitioning is consistent with previous work studying atmospherically relevant aldehydes, most notably glyoxal.

These results emphasize the importance of considering the gas–particle partitioning of atmospheric compounds based on their actual chemical form in the condensed phase, rather than their pure form in isolation. For the case of butenedial the current results suggest butenedial's $P_{\mathrm{vap,eff}}$ can be represented by a single value across all ambient RH.

The formation of intramolecular hydrogen bonds by hydrated butenedial may have a substantive effect on its volatility. Based on the structure of butenedial hydrate, the role of cis/trans isomerism is expected to play a role, with the cis form of butenedial dihydrate more likely to be able to form intramolecular hydrogen bonds and therefore demonstrate a high vapor pressure, compared to the trans form. Though the isomeric form of the precursor (cis) combined with the synthetic mechanism suggest synthesis of purely cis butenedial, evidence from our NMR spectra does not support this conclusion, instead suggesting our experiments were performed with a mixture of cis and trans isomers. However, we do not observe a double exponential shape to our evaporation data, which could imply either the vapor pressures of the cis or trans isomers do not have appreciably different vapor pressures, or the difference in evaporation rates is obscured by the noise in our data. Future studies on a wider set of compounds may help illuminate the effect.

The fact that $P_{\mathrm{vap,eff}}$ is invariant between the two RH conditions may imply in these experiments butenedial remained in its hydrated form even under dry conditions with little condensed-phase water. This may be due to butenedial being kinetically frozen as a hydrate over the experimental timescales of tens of minutes to hours. If this is indeed the case, the ability of our EDB-MS approach to determine butenedial's $P_{\mathrm{vap,eff}}$ is a consequence of butenedial hydrate evaporating over a timescale during which the dehydration reaction is negligible. This analysis points to the care that needs to be taken when considering the behavior of atmospheric aerosol. If using an experimental approach with appreciably different conditions from those reported here (e.g., temperature or butenedial concentration), the rates of the competing evaporation and dehydration pathways may exhibit different scaling dependencies and hence lead to a different conclusion about butenedial's behavior. One attractive quality of EDB-MS is it allows monitoring the evolution of a particle's composition over the multiday lifetime of an atmospheric aerosol particle. It is not necessary to use extreme experimental conditions to simulate some aspect of multiple days of atmospheric lifetime in a shorter period of time.

Observation of a higher $P_{\mathrm{vap,eff}}$ of butenedial in the presence of high concentrations of inorganic salts sodium chloride or sodium sulfate imply a salting-out effect that increased $P_{\mathrm{vap,eff}}$ of butenedial by up to a factor of approximately six to eight under the most concentrated inorganic conditions used in this experiment. In ambient particles the magnitude of the effect is expected to depend on the inorganic ion concentration, as described by the Setschenow coefficients. In general, the magnitude of the observed Setschenow coefficients is such that only with inorganic ion concentrations on the scale of >1 M is a significant effect predicted. The salting-out effect is predicted to be negligible with inorganic ion concentrations on the order of 100 μM to 1 mM. Consequently, the measured salting-out effect is predicted to have an influence on aqueous aerosol particles but not on cloud water. The magnitude and sign of the salting-in or salting-out effect is also known to depend on the identity of the ion, so further study would be necessary to investigate the effect of other inorganic ions. In general, better understanding of factors influencing gas–particle partitioning with this level of chemical detail improves predictions of the composition and fate of organic aerosol and its chemical constituents.

This work also helps inform the design of future experimental work using EDB-MS instrumentation. A measurement of particle diameter with lower uncertainty than the spring point technique would meaningfully reduce the uncertainty in extracted effective vapor pressures, particularly with a continuous diameter measurement. Other research with EDBs has demonstrated the utility of optical sizing techniques for performing this measurement (~~Zardini et al.,~~Gorkowski et al., 2018; Haddrell et al., 2012; Hargreaves et al., 2010; Marsh et al., 2017; Steimer et al., 2015; Zardini et al., 2006).

In sum, this work uses an EDB-MS laboratory technique to better understand the dependence of a model organic compound's effective vapor pressure on particle composition, and hence help contribute to an improved understanding of fundamental factors influencing gas–particle partitioning in atmospheric aerosol.

Data and code availability

The Python package pyvap used as the kinetic model of droplet evaporation is available at https://github.com/awbirdsall/pyvap. Data used to generate paper figures is available upon request.

Author contributions

AWB, JCH, and FNK designed the experiments. AWB and JCH performed the laboratory experiments and analyzed the data. PK and AJH developed the electrodynamic balance used to assess droplet efflorescence behavior. JCH developed the analytical solution approximating droplet evaporation and fitting procedure. AWB prepared the manuscript with contributions from all coauthors.

Competing interests

The authors declare they have no conflict of interest.

Acknowledgments

This material is based upon work supported by NSF grant CHE 1808084, the National Science Foundation Graduate Research Fellowship under grant numbers DGE 1144152 and DGE 1745303, and the Harvard University Faculty of Arts and Sciences Dean's Competitive Fund for Promising Scholarship. The authors thank Ulrich Krieger and Steven Wofsy for useful discussions.

References

Avenati, M. and Vogel, P.: Face selectivity of the Diels-Alder additions of 2-substituted 5,6-bis((E)-chloromethylidene)Bicyclo[2.2.2]Octanes, Helv. Chim. Acta., 65, 204–216, doi:10.1002/hlca.19820650119, 1982.

Bilde, M., Barsanti, K., Booth, M., Cappa, C. D., Donahue, N. M., Emanuelsson, E. U., McFiggans, G., Krieger, U. K., Marcolli, C., Topping, D., Ziemann, P., Barley, M., Clegg, S., Dennis-Smither, B., Hallquist, M., Hallquist, Å. M., Khlystov, A., Kulmala, M., Mogensen, D., Percival, C. J., Pope, F., Reid, J. P., Silva, M. A. V. R. da, Rosenoern, T., Salo, K., Soonsin, V. P., Yli-Juuti, T., Prisle, N. L., Pagels, J., Rarey, J., Zardini, A. A. and Riipinen, I.: Saturation vapor pressures and transition enthalpies of low-volatility organic molecules of atmospheric relevance: From dicarboxylic acids to complex mixtures, Chem. Rev., 115, 4115–4156, doi:10.1021/cr5005502, 2015.

Birdsall, A. W. and Elrod, M. J.: Comprehensive ~~no~~NO-dependent study of the products of the oxidation of atmospherically relevant aromatic compounds, J. Phys. Chem. A, 115, 5397–5407, doi:10.1021/jp2010327, 2011.

Birdsall, A. W., Krieger, U. K. and Keutsch, F. N.: Electrodynamic balance–mass spectrometry of single particles as a new platform for atmospheric chemistry research, Atmos. Meas. Tech., 11, 33–47, doi:10.5194/amt-11-33-2018, 2018.

Boucher, O., Randall, D., Artaxo, P., Bretherton, C., Feingold, G., Forster, P., Kerminen, V.-M., Kondo, Y., Liao, H., Lohmann, U., Rasch, P., Satheesh, S. K., Sherwood, S., Stevens, B. and Zhang, X. Y.: Clouds and aerosols, in: Climate Change 2013: The Physical Science Basis. Contribution of Working Group I to the Fifth Assessment Report of the Intergovernmental Panel on Climate Change, Cambridge University Press, Cambridge, United Kingdom, 2013.

Braun, C. and Krieger, U. K.: Two-dimensional angular light-scattering in aqueous NaCl single aerosol particles during deliquescence and efflorescence, Opt. Express, 8, 314–321, doi:10.1364/OE.8.000314, 2001.

Claflin, M. S. and Ziemann, P. J.: Thermal desorption behavior of hemiacetal, acetal, ether, and ester oligomers, Aerosol Sci. Tech., 53, 473–484, doi:10.1080/02786826.2019.1576853, 2019.

Cohen, A. J., Brauer, M., Burnett, R., Anderson, H. R., Frostad, J., Estep, K., Balakrishnan, K., Brunekreef, B., Dandona, L., Dandona, R., Feigin, V., Freedman, G., Hubbell, B., Jobling, A., Kan, H., Knibbs, L., Liu, Y., Martin, R., Morawska, L., Pope, C. A., Shin, H., Straif, K., Shaddick, G., Thomas, M., van Dingenen, R., van Donkelaar, A., Vos, T., Murray, C. J. L. and Forouzanfar, M. H.: Estimates and 25-year trends of the global burden of disease attributable to ambient air pollution: An analysis of data from the Global Burden of Diseases Study 2015, Lancet, 389, 1907–1918, doi:10.1016/S0140-6736(17)30505-6, 2017.

Compernolle, S., Ceulemans, K. and Müller, J.-F.: EVAPORATION: A new vapour pressure estimation method for organic molecules including non-additivity and intramolecular interactions, Atmos. Chem. Phys., 11, 9431–9450, doi:10.5194/acp-11-9431-2011, 2011.

Curry, L. A., Tsui, W. G. and McNeill, V. F.: Technical note: Updated parameterization of the reactive uptake of glyoxal and methylglyoxal by atmospheric aerosols and cloud droplets, Atmos. Chem. Phys., 18, 9823–9830, doi:10.5194/acp-18-9823-2018, 2018.

Davis, E. J.: Electrodynamic balance stability characteristics and applications to the study of aerocolloidal particles, Langmuir, 1, 379–387, doi:10.1021/la00063a021, 1985.

Dumdei, B. E. and O’Brien, R. J.: Toluene degradation products in simulated atmospheric conditions, Nature, 311, 248–250, doi:10.1038/311248a0, 1984.

Ervens, B. and Volkamer, R.: Glyoxal processing by aerosol multiphase chemistry: Towards a kinetic modeling framework of secondary organic aerosol formation in aqueous particles, Atmos. Chem. Phys., 10, 8219–8244, doi:10.5194/acp-10-8219-2010, 2010.

Gorkowski, K., Donahue, N. M. and Sullivan, R. C.: Emerging investigator series: Determination of biphasic core–shell droplet properties using aerosol optical tweezers, Environ. Sci.: Processes Impacts, 20, 1512–1523, doi:10.1039/C8EM00166A, 2018.

Haddrell, A. E., Davies, J. F., Yabushita, A. and Reid, J. P.: Accounting for Changes in Particle Charge, Dry Mass and Composition Occurring During Studies of Single Levitated Particles, J. Phys. Chem. A, 116, 9941–9953, doi:10.1021/jp304920x, 2012.

Hargreaves, G., Kwamena, N.-O. A., Zhang, Y. H., Butler, J. R., Rushworth, S., Clegg, S. L. and Reid, J. P.: Measurements of the Equilibrium Size of Supersaturated Aqueous Sodium Chloride Droplets at Low Relative Humidity Using Aerosol Optical Tweezers and an Electrodynamic Balance, J. Phys. Chem. A, 114, 1806–1815, doi:10.1021/jp9095985, 2010.

Hodzic, A., Aumont, B., Knote, C., Lee-Taylor, J., Madronich, S. and Tyndall, G.: Volatility dependence of Henry’s law constants of condensable organics: Application to estimate depositional loss of secondary organic aerosols, Geophys. Res. Lett., 41, 4795–4804, doi:10.1002/2014GL060649, 2014.

Hodzic, A., Kasibhatla, P. S., Jo, D. S., Cappa, C. D., Jimenez, J. L., Madronich, S. and Park, R. J.: Rethinking the global secondary organic aerosol (SOA) budget: Stronger production, faster removal, shorter lifetime, Atmos. Chem. Phys., 16, 7917–7941, doi:10.5194/acp-16-7917-2016, 2016.

Huisman, A. J., Krieger, U. K., Zuend, A., Marcolli, C. and Peter, T.: Vapor pressures of substituted polycarboxylic acids are much lower than previously reported, Atmos. Chem. Phys., 13, 6647–6662, doi:10.5194/acp-13-6647-2013~~:10.5194/acp-13-6647-2013,~~, 2013.

Ip, H. S. S., Huang, X. H. H. and Yu, J. Z.: Effective Henry’s law constants of glyoxal, glyoxylic acid, and glycolic acid, Geophys. Res. Lett., 36, L01802, doi:10.1029/2008GL036212, 2009.

Jacobs, M. I., Davies, J. F., Lee, L., Davis, R. D., Houle, F. and Wilson, K. R.: Exploring chemistry in microcompartments using guided droplet collisions in a branched quadrupole trap coupled to a single droplet, paper spray mass spectrometer, Anal. Chem., 89, 12511–12519, doi:10.1021/acs.analchem.7b03704, 2017.

Knote, C., Hodzic, A. and Jimenez, J. L.: The effect of dry and wet deposition of condensable vapors on secondary organic aerosols concentrations over the continental US, Atmos. Chem. Phys., 15, 1–18, doi:10.5194/acp-15-1-2015, 2015.

Krieger, U. K., Marcolli, C. and Reid, J. P.: Exploring the complexity of aerosol particle properties and processes using single particle techniques, Chem. Soc. Rev., 41, 6631–6662, doi:10.1039/c2cs35082c, 2012.

Krieger, U. K., Siegrist, F., Marcolli, C., Emanuelsson, E. U., Gøbel, F. M., Bilde, M., Marsh, A., Reid, J. P., Huisman, A. J., Riipinen, I., Hyttinen, N., Myllys, N., Kurtén, T., Bannan, T., Percival, C. J. and Topping, D.: A reference data set for validating vapor pressure measurement techniques: Homologous series of polyethylene glycols, Atmos. Meas. Tech., 11, 49–63, doi:10.5194/amt-11-49-2018, 2018.

Lide, D. R., Ed.: CRC handbook of chemistry and physics: A ready-reference book of chemical and physical data, 89th ed., CRC Press, Taylor & Francis, Boca Raton, U.S.A., 2008.

Lin, Y.-H., Zhang, Z., Docherty, K. S., Zhang, H., Budisulistiorini, S. H., Rubitschun, C. L., Shaw, S. L., Knipping, E. M., Edgerton, E. S., Kleindienst, T. E., Gold, A. and Surratt, J. D.: Isoprene epoxydiols as precursors to secondary organic aerosol formation: Acid-catalyzed reactive uptake studies with authentic compounds, Environ. Sci. Technol., 46, 250–258, doi:10.1021/es202554c, 2012.

Marsh, A., Rovelli, G., Song, Y.-C., Pereira, K. L., Willoughby, R. E., Bzdek, B. R., Hamilton, J. F., Orr-Ewing, A. J., Topping, D. O. and Reid, J. P.: Accurate representations of the physicochemical properties of atmospheric aerosols: When are laboratory measurements of value?, Faraday Discuss., 200, 639–661, doi:10.1039/C7FD00008A, 2017.

Nannoolal, Y., Rarey, J. and Ramjugernath, D.: Estimation of pure component properties: Part 3. Estimation of the vapor pressure of non-electrolyte organic compounds via group contributions and group interactions, Fluid Phase Equilibr., 269, 117–133, doi:https://doi.org/10.1016/j.fluid.2008.04.020, 2008.

O'Meara, S., Booth, A. M., Barley, M. H., Topping, D. and McFiggans, G.: An assessment of vapour pressure estimation methods, Phys. Chem. Chem. Phys., 16, 19453–19469, doi:10.1039/C4CP00857J, 2014.

Prisle, N. L., Engelhart, G. J., Bilde, M. and Donahue, N. M.: Humidity influence on gas-particle phase partitioning of α-pinene + O_3 secondary organic aerosol, Geophys. Res. Lett., 37, L01802, doi:10.1029/2009GL041402, 2010.

Pye, H. O. T. and Seinfeld, J. H.: A global perspective on aerosol from low-volatility organic compounds, Atmos. Chem. Phys., 10, 4377–4401, doi:10.5194/acp-10-4377-2010, 2010.

Seinfeld, J. H. and Pandis, S. N.: Mass transfer aspects of atmospheric chemistry, in: Atmospheric Chemistry and Physics, 2nd ed., John Wiley & Sons, Inc., Hoboken, USA, 537–587, 2006.

Shepson, P. B., Edney, E. O. and Corse, E. W.: Ring fragmentation reactions in the photooxidations of toluene and o-xylene, J. Phys. Chem., 88, 4122–4126, doi:10.1021/j150662a053, 1984.

Steimer, S. S., Krieger, U. K., Te, Y.-F., Lienhard, D. M., Huisman, A. J., Luo, B. P., Ammann, M. and Peter, T.: Electrodynamic balance measurements of thermodynamic, kinetic, and optical aerosol properties inaccessible to bulk methods, Atmos. Meas. Tech., 8, 2397–2408, doi:10.5194/amt-8-2397-2015, 2015.

Toivola, M., Prisle, N. L., Elm, J., Waxman, E. M., Volkamer, R. and Kurtén, T.: Can COSMOTherm predict a salting in effect?, J. Phys. Chem. A, 121, 6288–6295, doi:10.1021/acs.jpca.7b04847, 2017.

Topping, D., Barley, M., Bane, M. K., Higham, N., Aumont, B., Dingle, N. and McFiggans, G.: UManSysProp v1.0: An online and open-source facility for molecular property prediction and atmospheric aerosol calculations, Geosci. Model Dev., 9, 899–914, doi:10.5194/gmd-9-899-2016, 2016.

Wang, C., Lei, Y. D., Endo, S. and Wania, F.: Measuring and modeling the salting-out effect in ammonium sulfate solutions, Environ. Sci. Technol., 48, 13238–13245, doi:10.1021/es5035602, 2014.

Waxman, E. M., Elm, J., Kurtén, T., Mikkelsen, K. V., Ziemann, P. J. and Volkamer, R.: Glyoxal and methylglyoxal Setschenow salting constants in sulfate, nitrate, and chloride solutions: Measurements and Gibbs energies, Environ. Sci. Technol., 49, 11500–11508, doi:10.1021/acs.est.5b02782, 2015.

Welty, J. R., Wicks, C. E. and Wilson, R. E.: Fundamentals of momentum, heat, and mass transfer, 3rd ed., Wiley, New York, 1984.

Yu, G., Bayer, A. R., Galloway, M. M., Korshavn, K. J., Fry, C. G. and Keutsch, F. N.: Glyoxal in aqueous ammonium sulfate solutions: Products, kinetics and hydration effects, Environ. Sci. Technol., 45, 6336–6342, doi:10.1021/es200989n, 2011.

Zardini, A. A., Krieger, U. K. and Marcolli, C.: White light Mie resonance spectroscopy used to measure very low vapor pressures of substances in aqueous solution aerosol particles, Opt. Express, 14, 6951–6962, doi:10.1364/OE.14.006951, 2006.

Zuend, A., Marcolli, C., Luo, B. P. and Peter, T.: A thermodynamic model of mixed organic-inorganic aerosols to predict activity coefficients, Atmos. Chem. Phys., 8, 4559–4593, doi:10.5194/acp-8-4559-2008, 2008.

Zuend, A., Marcolli, C., Booth, A. M., Lienhard, D. M., Soonsin, V., Krieger, U. K., Topping, D. O., McFiggans, G., Peter, T. and Seinfeld, J. H.: New and extended parameterization of the thermodynamic model AIOMFAC: Calculation of activity coefficients for organic-inorganic mixtures containing carboxyl, hydroxyl, carbonyl, ether, ester, alkenyl, alkyl, and aromatic functional groups, Atmos. Chem. Phys., 11, 9155–9206, doi:10.5194/acp-11-9155-2011, 2011.

S1 Analytical solution to evaporation differential equation and curve-fitting procedure

To make the fitting procedure less computationally expensive, rather than repeatedly numerically integrating the differential equation we developed an analytical expression that approximates a closed-form solution to Maxwellian flux under certain simplifying assumptions. In particular, we assumed three quantities were time-invariant:

First, the droplet radius did not vary with time because the butenedial reflects only a fraction of the total droplet composition. For our experiments, the full numerical integration calculation showed particle radius decreased by less than 10% with complete butenedial evaporation and has a negligible effect on the vapor pressure calculation compared to overall uncertainty in our experiments.

Second, the mole fraction of water in the droplet did not vary with time. This approximation is true to the extent that the RH in the EDB remains constant and the change in composition over the droplet's residence of the EDB does not lead to a change in the activity coefficient of water.

Third, all components in the droplet that are not butenedial or water (i.e., PEG-6, NaCl and Na_2SO_4) did not evaporate over the timescale of the experiment.

Using these assumptions, it can be shown that the Maxwell flux expression can be simplified to

$$\frac{dN_i}{dt} = -a\frac{N_i}{b + cN_i} \qquad \text{(S1)}$$

where

$$a = 4\pi\frac{P_{\mathrm{vap,eff}_i} D_{\mathrm{g}_i} r}{kT} \qquad \text{(S2)}$$

$$b = \frac{1}{1 - X_{\mathrm{H_2O}}}\left(N_{\mathrm{PEG-6}} + N_{\mathrm{inorg}}\right) \qquad \text{(S3)}$$

$$c = \frac{1}{1 - X_{\mathrm{H_2O}}} \qquad \text{(S4)}$$

and N_i is the time-dependent number of molecules of compound i.

This form of differential equation has an analytical solution in the form:

$$N_i(t) = \frac{b}{c} W\left(\frac{c}{b} e^{-\frac{a}{b}t + \frac{C_0}{b}}\right) \qquad \text{(S5)}$$

where W is the Lambert W function and C_0 is an integration constant. From this solution it further can be shown that

$$C_0 = b\ln\left(N_{\mathrm{BD,(t=0)}}\right) + cN_{\mathrm{BD,(t=0)}} \qquad \text{(S6)}$$

The data was fit to Eq. S5 with the values of b, c, and C_0 constrained as input parameters and a as the free parameter whose value was determined via non-linear curve fitting. The fitting procedure used the Trust Region Reflective algorithm, which allows for fitting to an arbitrary function with parameters constrained to only take on physically meaningful positive values (Branch et al., 1999), as implemented in the SciPy scientific computing package (Jones et al., 2001–).

S2 Validation of analytical solution

The agreement between Eq. S5 and numerical integration was verified for our experimental conditions using the dry experiment because that is the experiment for which the largest change in droplet radius is expected to have taken place.

To confirm that the assumptions made in deriving the closed form solution to the Maxwell flux differential equation do not substantially affect the shape of the evaporation curve or the extracted vapor pressure, the closed form solution was compared to the best fit forward run of the Maxwell flux equation. Minimizing the root mean squared deviation (RMSD) of the forward model run from the observed butenedial evaporation was used as the metric to determine the forward run of best fit. As shown in Fig. S1 and Fig. S2, the best fit forward run was compared to the closed form solution for both the dry and humid measurements without inorganics present. In both cases, the vapor pressures converged to the same value within the uncertainty range, verifying that assuming constant radius, mole fraction of water, and nonvolatility of hexaethylene glycol does not alter the vapor pressure estimate significantly for the instrumental setup.

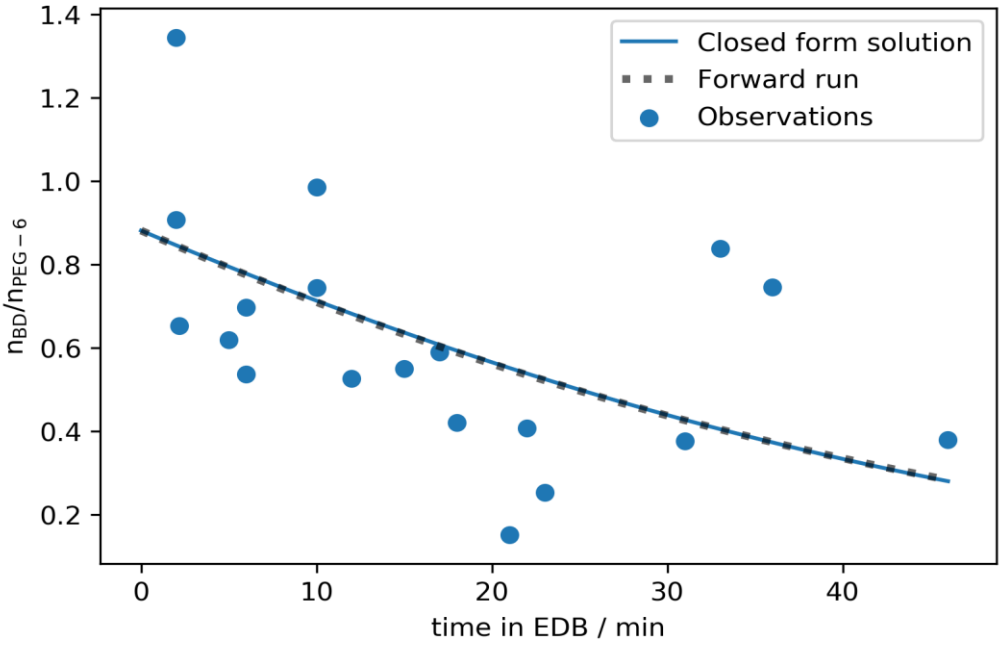

Figure S1: Validation of closed-form approximation, dry BD + PEG-6 experiment.

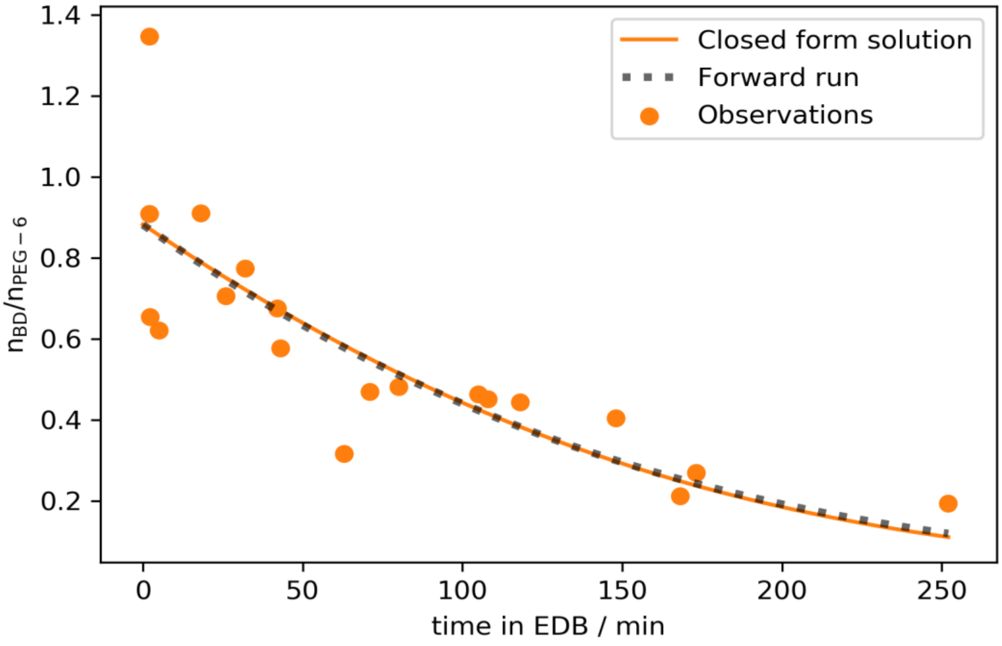

5 **Figure S2**: Validation of closed-form approximation, humid BD + PEG-6 experiment.

S3 Combined Monte Carlo and bootstrapping uncertainty analysis

The overall strategy of the combined Monte Carlo and bootstrapping uncertainty analysis was to obtain a distribution of extracted butenedial vapor pressures was obtained by repeating the fitting procedure in Sect. S1 10000 times, each time using a set of parameter values sampled at random from the set of distributions describing their uncertainties~~.~~ and an independently generated bootstrapped realization of binned data. The mean of the extracted butenedial vapor pressures provides a central value for the butenedial effective vapor pressure. The standard deviation describes the uncertainty due to uncertainties in the other model input parameters as well as ~~the standard error~~shot-to-shot noise in the ~~model fit coefficient~~data.

The source of the uncertainty in diameter arises from a combination of inherent uncertainty in the measurement and droplet-to-droplet variability, though the characteristics of each droplet were kept as consistent as possible. The uncertainties in gas-phase diffusivity and scaling factor reflect uncertainties in the underlying parameters, rather than reflecting any variability in the values from particle to particle. The uncertainty in temperature does reflect the extent to which the EDB temperature drifted with time, though it should be noted the effect of temperature on the evaporation model over this range is limited. Each input parameter was represented by a Gaussian distribution centered at the mean value and with standard deviation based upon the variability or uncertainty in its measurements. The Monte Carlo approach assumes independence between each of the model input parameters, which is a reasonable assumption for this set of parameters. The distribution of each input parameter was treated separately for each experiment type (i.e., dry, humid, NaCl #1, NaCl #2, Na_2SO_4).

For each type of experiment, we binned the data into different time periods: those for which the time residing in the EDB was approximately 0 minutes, and then a series of equally spaced bins such that a total of 4 time bins were obtained. For each of the 10000 repetitions of the model fitting procedure, a bootstrapping procedure was used within each time bin to generated a bootstrapped realization of the normalized signal response. The model was fit to the mean value of the bootstrapped data within each time bin. The data was scaled for each trial assuming the bootstrapped mean for the "t=0" bin represents the initial normalized molar abundance of butenedial relative to the internal standard.

To calculate $P_{\text{vap,eff}}$ for each iteration of the Monte Carlo technique, a ~~value~~95% confidence interval of a was ~~used~~estimated using the interval that ~~accounted for the standard error in~~encompassed the~~ value of a~~ extracted ~~from the curve-fitting procedure. A single value of a was sampled from a standard distribution centered at the optimal estimate of a, arising from the current iteration of curve-~~model fit for 95% of the 10000 model fitting ~~procedure, and with standard deviation equal to the square root of the variance of the a estimate, again from the current iteration of the curve-fitting procedure.~~trials. Using this ~~sampled value~~95% confidence interval of a in Eq. S2, ~~the value~~a 95% confidence interval of P_{vap} was calculated~~ for a single iteration of the Monte Carlo technique~~.

References

Branch, M. A., Coleman, T. F. and Li, Y.: A subspace, interior, and conjugate gradient method for large-scale bound-constrained minimization problems, SIAM J. Sci. Comput., 21, 1–23, doi:10.1137/S1064827595289108, 1999.

Jones, E., Oliphant, T., Peterson, P. and others: SciPy: Open source scientific tools for Python, [online] Available from: http://www.scipy.org/ (Accessed 23 February 2019), 2001–.